Research Article

Riaz A. Khan* and Azra J. Khan

# Miniaturized peptidomimetics and nano-vesiculation in endothelin types through probable nano-disk formation and structure property relationships of endothelins' fragments

https://doi.org/10.1515/ntrev-2022-0022
received November 19, 2021; accepted December 18, 2021

**Abstract:** Endothelins (ETs), which are multi-functional-peptides with potential for antagonist-based-therapy in various physiological-malfunctionings, including cardio-vascular, nephrological, oncologic, and diabetic conditions, may produce newer chemical entities and drug leads. The present study deals with molecular-modeling of the ETs' sub-types, ET-I, II, and III to find the structure property-relationship (SPR) of the ETs, and individual fragments derived from the ET sub-type ET-I. The ETs peptidic tails' amino acid (AA) sequence's structural differences and similarities, various dissected fragments of the ET-I, and SPR comparison with the sarafotoxin-6b (SRT-6b), a structurally-related snake-venom, showed points of dissimilarities for their structural specifications, geometric disposition, and physico-chemical properties. The generation of miniaturized (shortened sequence) peptides towards offering peptidomimetic compounds of near- and far-values compared SPR with estimations for log *P*, hydration energy, and other molecular and quantitative structure activity relationship (QSAR) were based on random and ordered-fragments derived from the original ET-I AA's sequence, and sequential distance changes in the original ET-I sequence's chain of 1–21 AA. The feasibility of alternate and bond length parameters-based possible cysteine–cysteine cyclizations, sequence homology, AA's positional demarcation, and presence/absence of cysteines, homology-based basic non-cysteine and cysteines-AA based cyclization, total structure and fragments end-to-end cyclizations, and geometrical analogy-based miniaturized sequence of the shorter AAs from the original ET-I sequence, together with mutated replacements with naturally constituent AAs of the ETs, and SRT-6 sequences were utilized. The major findings of the fragmented sequences, and sequences at par with the

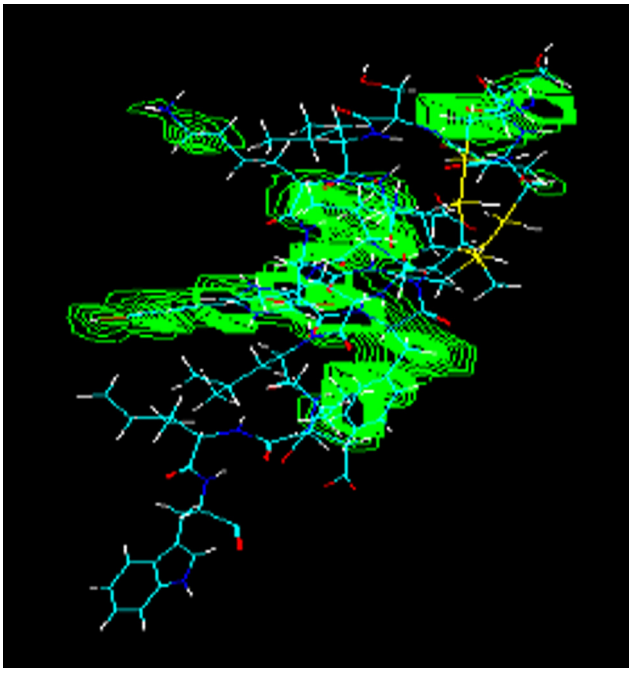

**Graphical abstract:** The present study deals with the molecular modeling studies of the endothelins (ETs), a multi-functional 21 amino acid (AA) peptides, with sub-types ET-I, II, and III to find the structure property relationship (SPR) of different fragments naturally derived from the cyclic body part of the ETs' structures together with the structurally similar and common tail sequence (AA 16–21) utilization of the ETs and the dissimilar sarafotoxin-6b (SRT-6b) hexapeptide chain tail, as well as their SPR comparisons to find peptide-based leads as comparable to the ETs, especially ET-I. Approach to plausible vesiculation of the ETs and the involved process as a suggested mechanism is also discussed.

*** Corresponding author: Riaz A. Khan,** Medicinal Chemistry and Pharmacognosy Department, College of Pharmacy, Qassim University, Qassim 51452, Saudi Arabia,
e-mail: ri.khan@qu.edu.sa, riaz.a.kahn@gmail.com
**Azra J. Khan:** Department of Chemistry, Kamala Nehru Institute of Science and Technology, Sultanpur, UP, 228118, India,
e-mail: jamal.azra400@gmail.com

original ETs to provide structures similar to the size, volume and with molecular and electronic properties of electrostatic potential and total charge density distribution, crucial factors in receptor bindings were investigated. The SPRs, molecular properties, and QSAR values were estimated to compare and validate the findings with the known homologous compounds, ET-I, and its known and potent antagonists. The study resulted in leads of smaller and larger sizes of peptide-based compounds which may have prospects as potent antagonist and in future needs their bioactivity evaluations after the synthesis. Moreover, approach to plausible vesiculation of the ETs, and the involved processes and structural requirements, together with the molecular interactions in settling a nano-vesicle of the peptidic structure with a possible mechanism is also suggested.

**Keywords:** endothelins, sarafotoxin-6b, structure property relationships, compartmentalization, miniaturized peptide, peptidomimetics, vesiculation

# 1 Introduction

The endothelin family of peptides, collectively termed as endothelins (ETs), comprises of endothelin-I (ET-I), endothelin-II (ET-II), and endothelin-III (ET-III), with binding to at least four different known endothelin receptors, *i.e.*, $ET_A$, $ET_{B1}$, $ET_{B2}$, and $ET_C$ in the biological system [1,2]. The ETs have varying regions of distribution in biological sites [3], and are produced by vascular endothelium through pre-pro-ETs resulting in 39 amino acids (AAs) precursor, big ETs, which is transformed through activities of endothelin converting enzyme located on the endothelial cell membranes into various ETs (Figure 1) [4–7]. The ETs and its receptors have been cloned [8–10] and molecularly characterized [11]. Various peptidic and non-peptide receptor antagonists have also been designed and synthesized for therapeutic evaluations since its discovery in 1988 [12–20]. However, the structural generality, non-specificity, and preferential ligand binding of the

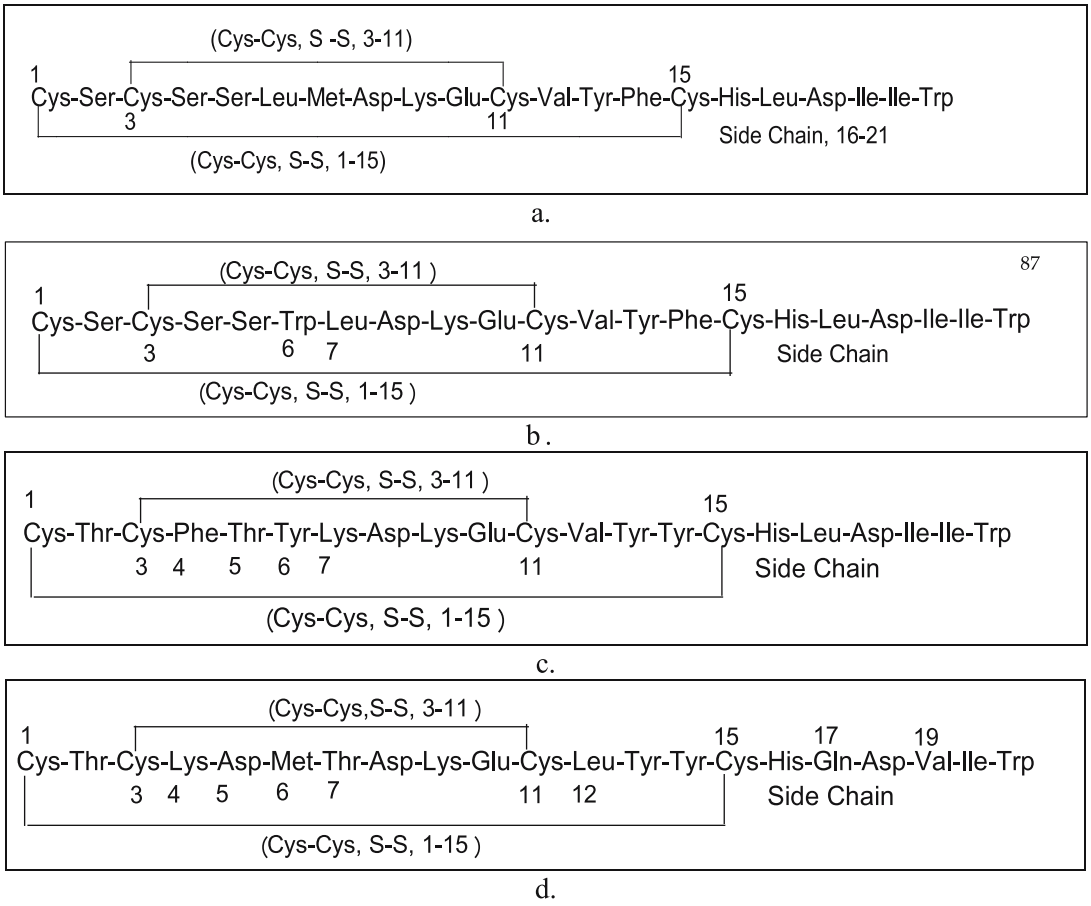


**Figure 1:** ETs; (a) ET-I, (b) ET-II, (c) ET-III, and (d) SRT-6b.

endothelin receptors, *i.e.*, $ET_A$ and $ET_B$ types, cross-talk, common/multiple-bindings, and cross-reactivity, seemingly, subdued the progress in the ET-based therapy developments. Interestingly, the endothelin receptor types ($ET_A$, $ET_{B1}$, and $ET_{B2}$) mediate ETs regulatory actions, and the ET-I, being the biologically most potent and predominant member of the endothelin peptide family, preferentially binds to $ET_A$ receptors, whereas the $ET_B$ type receptors entangle both the ET-I and ET-III peptides [21]. The $ET_B$ receptor type/ET-III axis is also considered as an endogenous "antagonist" system of the body opposing the effects of $ET_A$/ET-I mediated bioactivities. The $ET_B$ receptor types mediate both the vasoconstriction and vasodilation activities in different tissues and organs, and seem to be have an elaborate, though probably non-specific, restricting control mechanism. Therefore, the selective $ET_A$ antagonist development for therapeutic applications have been preferentially taken up from the drug discovery viewpoint, involving the non-peptidic or mixed peptidic structural components, pharmacophore mapping, peptidomimetic variants, and alternates of known antagonists more frequently, and more recently [22–26].

The ET's $ET_A$-receptor has been found to be responsible for growth promotion and pro-inflammatory activities which are responsible for developing chronic diseases, *i.e.*, atherosclerosis, hypertension, renal malfunctions, and heart failure, primarily owing to the elevated ET-I levels [27,28]. The ETs, which are potent vasoconstrictor peptides, are also considered to be associated with several other diseases of lungs, kidneys, vascular system, reproductive organs, nervous system, heart failure, and cancers. These ETs are expressed ubiquitously by the stress-responsive regulators with both beneficial and detrimental effects, specifically with the ET-II and ET-III isoforms [29–32]. The diseases associated with cell growth and inflammatory activation, *i.e.*, arterial hypertension, glomerulo-sclerosis, and immune mediated malfunctions involving cancers, connective tissues ailments, and chronic allograft rejections, as well as metabolic diseases of obesity and diabetes, are turning to be renewed challenges for developing endothelin-antagonist-based therapies [33,34].

Several studies have thus led to the discovery of selective $ET_A$ receptor antagonists (including non-selective $ET_A$ and $ET_B$ antagonists) and pharmacophore optimization for the purpose [35]. The preclinical and clinical studies have clearly established that these antagonists are effective in treatment of essential hypertension, pulmonary hypertension, heart failure, and atherosclerosis [36–40]. Advances in this area resulted in the US-FDA approval of the first orally active antagonist Bosentan followed by Ambrisentan for pulmonary hypertension and vasoconstriction [41,42]. However, the role of anti-endothelin therapy in the treatment of cardiovascular and other diseases, and determinations of the roles of the selective receptor antagonism vs mixed $ET_A/_B$-receptor(s) antagonism in human diseases, certainly needs further elaboration from the structure activity relationship and structure property relationship (SAR and SPR) viewpoints.

The SAR studies on the structural requirements of ET-I to exhibit pressor and depressor responses are available. The oxidation of the methionine amino acid at position-7, $Met^7$, resulted in retained hypotensive activity of the analog, while the removal of the natural $Cys^1$–$Cys^{15}$ disulfide bridge led to weak agonistic action with both the pressor and depressor types' activities of the ET-I analog. The formylation of terminal $Trp^{21}$ amino acid resulted in complete loss of the activity. These results indicated that $Met^7$ and the indole moiety of the $Trp^{21}$ are important structural requirements for the expression of activity of ET-I, whereas the intramolecular loop structure, the cyclized part, is less important. The study also provided further evidence that the depressor and pressor effects of the ET-I are mediated through different receptors [43]. The $Asp^{18}$ and $Ile^{19}$ AA residues replaced by alkyl spacers of various (chain) lengths of the C-terminal analog, Ph–Ph–$CH_2$–O–N═CH–CO–Phe–Asp–Ile–Ile–Trp–OH, proved the role of the central portion of the ET-I sequence, and helped to identify the N- and C-terminals as pharmacophoric regions of the ET-I sequence. The side-chains of the centrally located peptide have been shown to be irrelevant for the binding of the molecule to the receptor but the distance between the two postulated sites for the interaction of the ligand with the $ET_B$ receptor have been found to be of fundamental nature for bindings, and consequently, activity exhibitions [44].

These preliminary studies have opened up the ETs sequences for more scrutiny and newer developments in understanding of the SARs of the peptidic and non-peptidic analogs by various groups. Among the non-peptidic analogs, the sulfonamides, biphenyl sulfonamides [45,46], 4-sulfonamido-pyrimidines [47], azoles [48–50], and indan derivatives, as endothelin antagonists [51], including atrasentan (ABT-627)-based pyrrolidine-3-carboxylic acids[12], have been designed, prepared, and bioactivity evaluated. Among the peptide analogs, the tripeptide antagonists with unnatural AA have showed that the first AA, in the sequence, need to have a high dependency for hydrophobic residues, while the second AA can be aromatic hydrophobic AA, and the third AA must be a D-isomer as part of the minimum pharmacophore requirements based on the stereo-electronic and conformational dependency [52]. The observation that the sequence heterogeneity at the N-terminal portion of

AA from positions 4–7 showed marked biological activity differences between ETs, and SRT-6b further confirmed the role, outreach, position, and spacing importance of each of these AA. The fact that the vasoconstrictor activities of the ET-II, ET-III, and SRT-6b have been found to be one-half, one-60th, and one-third of that of the ET-I, respectively, the structural heterogeneity as well as sequence isosteric nature and homogeneity/similarities, which are well pronounced and confirmed with defined and definite levels of biological activity of the ET-I, ET-II, ET-III, and SRT-6b analogs, are proof of the concept [53]. The fact that the physico-chemical properties and molecular attributes of these molecules affected their receptor selectivity, receptor binding extents, and affinity, and the biological activity exhibitions have made them a prime target for SAR and SPR studies [54]. Moreover, a monocyclic ET-I analog, devoid of $Cys^3$ and $Cys^{11}$ AA which were replaced by Ala and Ala AA, had showed one-third of the activity of the ET-I, while the diamino, dicarba analog turned out to be nearly inactive, thereby indicating the role of the termini groups. However, no significant changes were observed in major bioactivities of the isoform ET-I with replacements of $Ser^4$, $Ser^5$, $Leu^6$, $Met^7$, $Lys^9$, $Tyr^{13}$; $Trp^{21}$ by Ala, Ala, Gly, Met(0), Leu, Phe; and Tyr or Phe, respectively. On the other hand, the replacement of $Asp^8$, $Glu^{10}$, and $Phe^{14}$ by Asn, Gln, and Ala, respectively, resulted in complete loss of the biological activity. These results indicated that the two disulfide bonds in ET molecule are not essential for the expression of vasoconstricting activity, but both the terminals' amino and carboxyl groups, carboxyl groups of $Asp^8$ and $Glu^{10}$, and the aromatic group of $Phe^{14}$ seemed to be contributing to the receptor binding and expression of the biological activity, and thus, seemed to be essential for the activity manifestation [55]. Yet, in another approach, tripeptides composed of unnatural AA, namely, linear peptide derivative, BQ-485, perhydro-azepin-1-yl-l-leucyl-D-tryptophanyl-D-tryptophan resulted in potent anti-contracting activity. The HIM-CO–Leu-D-Trp-D-Phe-(–R)-OH compounds as $ET_A$ receptor antagonists provided a tool for the development of therapeutic agents in the treatment of ET-I manifested disorders [56]. The study by Kimura *et al.* [57] established the importance of the C-terminal AA, wherein replacement of $Trp^{21}$ with D-Trp, reduction and carboxamido methylation of the four Cys residues, and cleavage at $Lys^9$ significantly lowered the vasoconstriction activity of the ET-I analogs. Further, studies on hexapeptide derivatives [58], linear tripeptide derivatives, $R_1R_2$·NC(O)–Leu-D-Trp-β-Ala-OH, derived from endothelin antagonistic cyclic-pentapeptide, BQ-123 [59], peptidomimetic analog containing p-Cl–Phe [60], and combinatorial synthesis for the optimization of the potent ET-I analogs [61], are available [62]. The $ET_B$ receptor antagonists, BQ-788 [*N-cis*-2, 6-dimethylpiperidinocarbonyl-L-γ-methylleucyl-D-1-methoxycarbonyltryptophanyl-D-norleucine] [63] further provided the required insight into the structural requirements for the bioactivity generation, the details of which could be utilized in understanding the roles of the ETs in physiological and pathological processes.

The current study focusses on a combination of approach dealing with the SPRs of various ETs isoforms, including the effects of naturally mutated AA-based analogs, miniaturized ET analogs in ET-I, as an example applicable to, in approach, to ET-II and ET-III, since ET-I is the most potent isoform. These isoforms were studied for their molecular properties, and molecular size due to the different sequence patterns. The sequences were downsized to new structures based on the ET-I together with the SRT-6b peptide, the snake venom toxin, which has been instrumental in providing a marked differentiation for receptor affinity, and its binding preferences to the ETs receptors. The observation by earlier researchers reported that the ETs are capable of modulating the biological action in so many of the body tissues and organs prompted to undertake the thorough and dissecting analysis of the sequences of ET-I isoform, and predict their effects on the possible SPRs, which also need to be validated through appropriate receptor-binding and *in vivo* experimentations, in addition to the *in silico* experimentations and prediction studies. However, the current study focuses on the computational modeling, molecular properties and QSAR value estimations in relation to the designed sub-peptidic structures. The study also proposes the nano-scale vesiculation process as part of the plausible mechanism and role of several factors of extracellular surroundings, media, pH, structural specifications, *etc*.

## 2 Materials and methods

The molecular modeling was performed on Hyper-Chem v 7.5 (Hypercube Inc., Gainesville, FL, USA), and Advanced Chemistry Development (ACD) Freeware, Ontario, Canada. The *in silico* generated peptide models obtained from ET-I, II, III, and SRT-6b peptide sequence structures' manipulation, shortening, and dissection were designed. A set of approaches were consulted [29,41,64–68]. The exercise provided different cyclic peptides of varying length where the cyclizations between the $Cys^1$, $Cys^3$, $Cys^{11}$, and $Cys^{15}$ have been made with several different combinations of the

cyclization between these Cys residues, while the ET's tail sequence was utilized as addendum to these designed cyclic structures to provide models of different sequences. All the structures were predicted for their calculated molecular and QSAR properties, and the comparisons of the properties and molecular attributes were made. The conformation linked energy minimizations through "steepest descent algorithm" in Hyper-Chem v 7.5 was performed. The most stable structure arrangement and the molecular geometries were predicted, which were sorted out for further analyses of physico-chemical characteristics and QSAR properties relationship. In order to get an empirical idea, and find rationalizations about the energy levels and behavior of the different peptide fragment models, molecular energy was minimized to get the stable and minimum energy conformation thereof. The most energetically favorable models were obtained and studied. On the outset, the minimum energy conformations of various fragments were compared to know the extent of changes in the physico-chemical properties of the fragments. All the molecules and their start set-up were simulated at 0.01 Å/cycle through 1,000 cycle's calculations. The predictions for molecular properties were estimated (atoms exhibiting non-parametric characters were opted to be ignored in the software based calculations), and molecular volume, total charge density, and electrostatic potentials of the fragments, their log *P*, and hydration energies were calculated.

# 3 Results and discussion

## 3.1 Optimization of ETs, SRT-6, and sequence fragmentations: Approach and design

The ETs, naturally encountered as ET-I, ET-II, and ET-III isoforms, with differentiating sequences were primary structures to begin with. Interestingly, all types of endothelin's tails have major sequence similarities with the snake venom toxin, SFT-6b sequence, but lacked the commonality of the biological activity with either being inactive, strongly active, diminished, or different activities. The study pursued to generate and rationalize the design of new structures through permutation and combination approach of the AA sequence to reach the best and optimized structure for further development. The structural similarities and differentiating points were considered in the design.

## 3.2 Tail and cyclic portions' analysis of the ETs and SRT-6b: Activity and property implications

For all the ETs, ET-I, ET-II, and ET-III, the hexapeptide tail sequence of AAs located from position 16–21 (single letter code sequence; HLDIIW) is similar, and is suggested to be structurally insignificant in terms of demarcation in receptor binding for biological activity elicitations; although, it has been suggested that the C-terminal hexapeptide chain discriminates between the different endothelin receptors [69]. Since this tail is similar in sequence structure for all the endothelin sub-types, the possibility for it to be distinguishing between receptor sub-types is remote. Any possibility of distinction between the receptor sub-types by the tail lies in the tail adopting different conformations and being distinctively different in the surroundings for differentiating the various receptor domains with the stereo-orientation assisted and modified by the (nearly common) cyclic part of all the ETs' sub-structures. Hence, the cyclic part of the structure may also play an important role in distinguishing the different receptor sub-types, and there is strong probability of it to do the major part in this exercise. The major AA-based structural differences of the main body cyclic part of the ETs is in the AA sequence for positions 2, 4, 5, 6, and 7. The differing AAs are Leu and Met at positions 6 and 7 of ET-I, which are replaced by Trp and Leu AA-residues, respectively, at position 6 and 7 for the ET-II, while the ET-III is completely different by the presence of Thr, Phe, Thr, Tyr, and Lys at 2, 4, 5, 6, and 7 positions of the AA sequence of its structure. However, the snake venom toxin, SRT-6b, also a 21 AA hexapeptide chain, have a different AA sequence structure as compared to that of the ETs tails (AA 16–21). For the cyclic structure part, few common AAs are available in the sequence for SRT-6b, otherwise it is largely different in its structure. This is an intriguing structure similarity/dissimilarity, seemingly, responsible for venom's extreme cardiovascular inhibitory activity [70–72].

## 3.3 Peptide foldings, compartmentalization, and mutated AA: Geometric views

The main body cyclic sub-structure of SRT-6b differs from ET-I by AAs located at positions 4–7 and 12, and replaced AAs are identified as Lys, Asp, Met, Thr, and Leu. The Leu at position 12 in SRT-6b is occupied by Val in the ETs'

sequences. The SRT-6b is also known to interact and involve in competitive binding with ETs [73]. Therefore, the point of interest for the AA sequence in SRT-6b is the tail composition which is, supposedly, also responsible for the demarcation between endothelin receptor types in ETs structures. The AA positions at 17 and 19 in all ETs are filled by the Leu and Ile AA residues, while the same slot is occupied by Gln and Val in SRT-6b molecular compositions. However, with the presence of different receptors in ileum and cerebellum [74], this observation further confirmed the presence of different ET types on structures' basis. It may also be considered that different structural domains formed from the molecular interaction and aggregation of the structures in the surrounding areas give rise to distinct compartmentalization, in their interaction area, when interacting with outside moieties, especially, water and other smaller entities, *e.g.*, ions and atoms in the structures, pH, media polarity, surface, and molecular entities' interactions of hydrophilic and hydrophobic nature. The axis-based alignments in the molecule in response to the external and internal factors and interactions help to formulate the compartment (Figure 2). The compartmentalization seemingly is facilitating the approach to binding, and enhancing the competitive binding by providing a different look in peptidic folding and its conformations to the ETs and SRT-6b receptors.

## 3.4 Molecular properties and QSAR attributes: SPR and SAR

The presence and interactions of singular molecular water, and water as part of the cluster, ions, and other small molecules at certain specified locations in the receptor area, along with the participation of inorganic, and/or other non-proteinaceous organic ligands, as well as the receptors maneuvering the binding feasibility even by difference of a single AA in the structures of SRT-6b and ETs may be very crucial. The physicochemical factors are vital and play significant roles at receptors' interaction levels. The hydrophilicity, hydrogen binding, hydrophobicity, and electronegative characteristics of the atoms, total charge density and its distribution on the molecule, as well as the

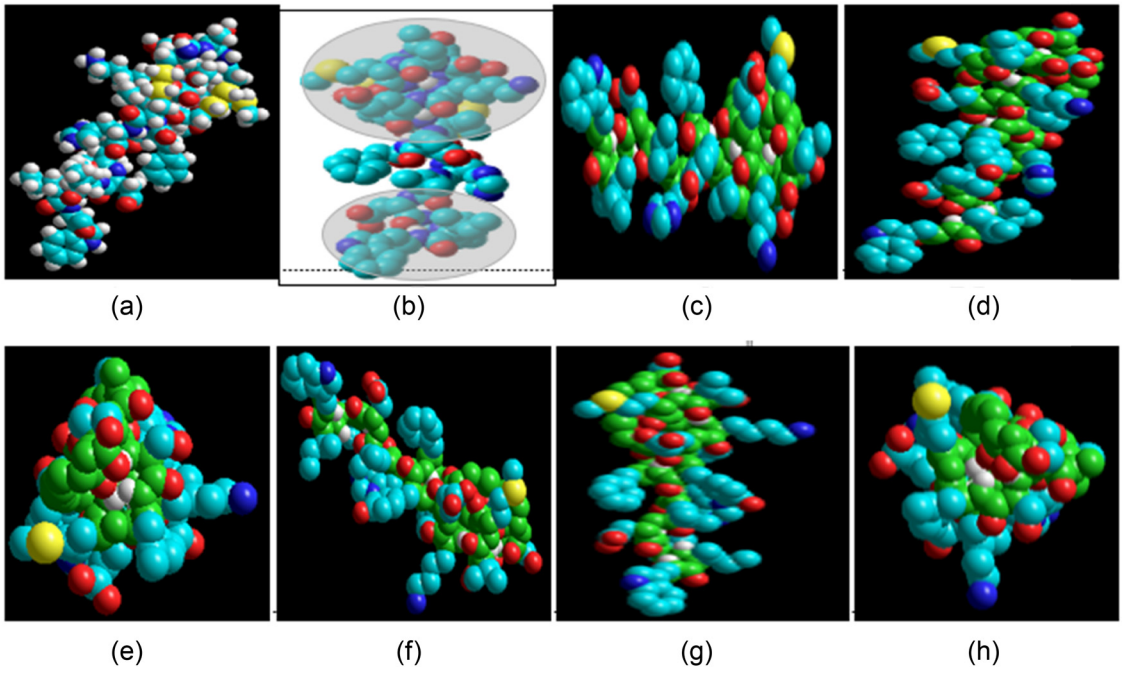


**Figure 2:** Peptide folds, ET-I based with compartmentalization, and the sequence's geometries: Emerging structural orientations with resultant geometry and axial alignments of the molecule providing different views of the geometry, with all the back-bone atoms in the models appearing as green atoms; (a) molecule leading to compartmentalization, shown with the explicit hydrogen atoms; (b) nearly three distinct major regions are appearing; (c) primary *X*-axis alignment; (d) *Y*-axis alignment; (e) primary *Z*-axis alignment, probably for passage through channels; (f) secondary *Y*-axis alignment; (g) secondary *Z* axis; (h) tertiary *X* (as major axis), primary *Y* axis orientation. Structures are shown without explicit hydrogens, the space-filling models' explicit hydrogens are white, the carbon atom is magenta colored, oxygen is red, nitrogen blue, and sulfur is yellow colored, the color scheme follows the current and all the subsequent models, unless otherwise stated.

electrostatic potential on structural parts and fragments, are some of the parameters to look for. The parachor, index of refraction, surface tension, density, and ring double bond equivalent (RBDE), of which the later is representative of the levels of unsaturation in the molecule and their fragments, and perhaps is being considered in the software pediction to indicate for the hydrophobic character contribution, which is prominent in receptor binding interactions. These predictors are also important to look for from different perspectives of the molecular properties of the structures. The QSAR molecular attributes predicting polarizibility, refractivity, log *P*, hydration energy, and molecular volume are other factors suggestively forming the SAR/SPR of different ET types, and the receptor demarcation activity by these ET motifs is pursued by the molecular properties in conjunction with the QSAR predictors. The prepared monocyclic fragment analogs of ET-I for exploring the importance of the bicyclic structure of ET-I to its predictive molecular and electronic properties showed low micro to high nano-molar binding affinities, and were functional antagonists of ET-I for induced accumulation of inositol phosphates. However, one analog possessed mixed antagonist/agonist activity at the two ET receptor subtypes [75–77]. The current work involved the *in silico* modeling and generated analogs of the ETs. The mapping of ET-I showed the 2D contour graph for the total charge density and electrostatic potential localized in the cyclic structure part of the molecule, which apparently was suggested as inactive, while the common to all ET was the tail sequence (AA 16–21). Hence, from the viewpoint of design and *in silico* study, the cyclic structure part needed more elaborate understanding to distinguish between the receptor sub-types, which is evident from their differing bioactivity and receptors' affinities. On comparing the molecular attributes and QSAR data (Table 1) for ETs and SRT-6b, the log *P* and hydration energy differences are remarkable, while other characteristics and QSAR properties also differ, interdependent of their structures. The structures of the ET-I, II, III, and SRT-6b are represented in Figure 3. The ET-I molecular modeling based electrostatic potential was predicted high, mainly localized in the loops (S–S bonds and non-tail AA 16–21 area of the structure), while the total charge density was moderate and distributed in the similar regions as that of the ET-I's electrostatic potential. The ET-II exhibited high electrostatic potential and high total charge density distributions, both being more than the ET-I, while the ET-III showed lesser electrostatic potential and total charge density than the ET-II but more than the ET-I. The SRT-6b exhibited these molecular characteristics nearly equal to ET-III. Of the ETs, the ET-I being most potent of the ETs, the high electrostatic potential and medium levels of charge density seemed to be favored for ET-I functions, and an antagonist activity elicitation is expected to be triggered through the competitive binding.

**Table 1:** Molecular attributes and QSAR properties of the ETs and SRT-6b*

| Property | ET-I | ET-II | ET-III | SRT-6b |
|---|---|---|---|---|
| Molar refractivity | 629.50 | 648.98 | 676.06 | 641.30 |
| Molar volume | 1,957.0 | 1,979.7 | 2,056.30 | 1,974.80 |
| Log *P* | 4.98 | 7.95 | 9.03 | 5.40 |
| Hydration energy | −40.20 | −47.61 | −57.28 | −57.79 |
| Parachor | 5,227.60 | 5,335.2 | 5,564.16 | 5,339.66 |
| Index of refraction | 1.556 | 1.569 | 1.571 | 1.562 |
| Surface tension | 50.9 | 52.7 | 53.6 | 53.43 |
| Density | 1.273 | 1.286 | 1.285 | 1.298 |
| Polarizability | 249.55 | 257.27 | 268.01 | 254.23 |
| RDBE | 43 | 49 | 51 | 45 |

*Molar refractivity expressed as $Å^3$ (cubic Angström), volume as $Å^3$, hydration energy in kcal/mol, density in $g/cm^3$, surface tension in dyne/cm, parachor as $Å^3$, polarizability as $Å^3$; insignificant variations have been omitted. The log *P* and hydration energy were predicted from Hyper-Chem 7.5, and rest of the properties were calculated from the ACD software.

## 3.5 Role of Cys residues, sequence shortening, and miniaturized ET: Dissection of the big ET

The big ET sequence of 38 AA was miniaturized to smaller 21 AA sequence to render the required biological activity. The elicitation is naturally possible after cleavage of the Trp–Val (21–22 AAs) bond by protease enzyme, and the biological activity is dependent on the cleavage process, and proceeds as the intermediate action, which is facilitated physico-chemically. Interestingly, the 22–38 AA sequence for human ET-I contains no Cys residue. The small ETs sequence stabilize them by attaching to other ligand through physical interactions, which provides physiochemical changes necessary to elicit the biological response when interacting with the receptor. However, it was also decided to take an approach to find the minimum sequence possible for the ET-I on the 21 AA sequence, and permute and combine sequences for finding a smaller possible sequence to entail the 16–21 AA residues to it, and produce a mini ET sequence equivalent to ET-I as a template by inducing the sequence optimization as described in structure dissecting approach. The energy diagram, electrostatic potential, and other comparative molecular attributes were also predicted.

## 3.6 Cavity modeling, Cys–Cys bonds, hydrogen bondings: Evolution of electronically active part

The backbone comprising the α-carbons of the AAs and the amide bonds were modeled for their minimum energy conformation (MEC) energy conformations based geometric orientations (Figure 4). All the 21 AAs produced a tailed cavity and AAs 1–15 were part of the cavity (Figure 4c), while the tail sequence AA 16–21 were not in the cavitation, and the atoms on the backbone are visualized in Figure 5. The structural stacking (overlaps) and geometric changes were facilitated by the energy requirements, and the Cys–Cys bondings of the ET-I molecule (Figure 6), hydrogen bonding effects, and internal axes from 1–2 and 3–4 showing the atoms and the residues distribution ratio in the ET-I molecule along the back-bone (shown as broken lines other than the hydrogen-bondings),

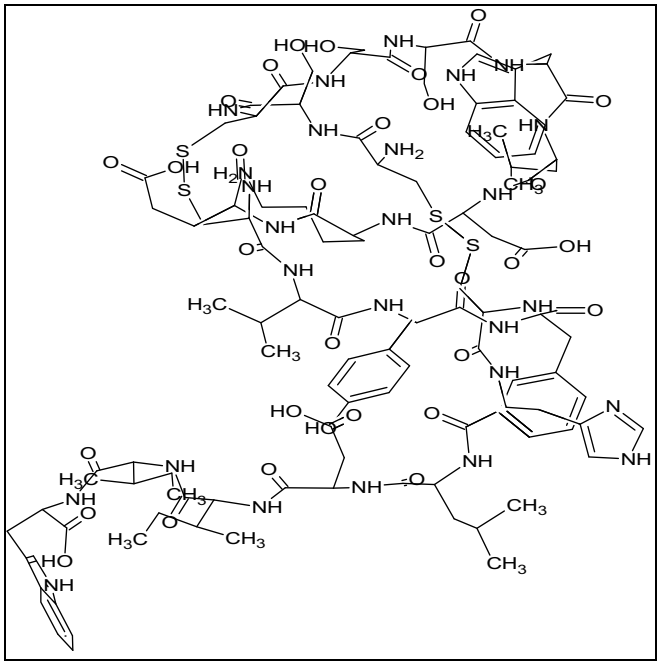

a)

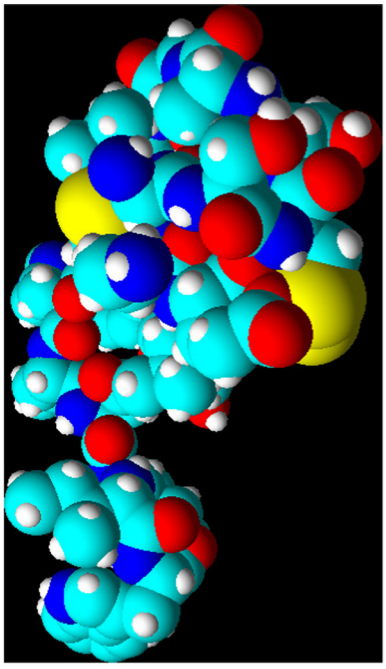

b)

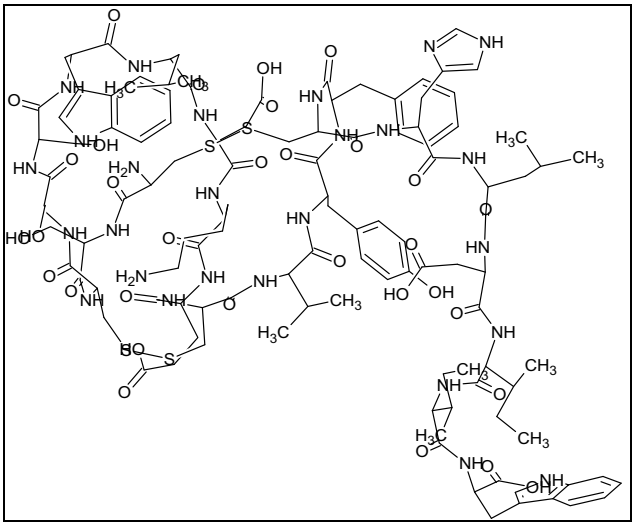

c)

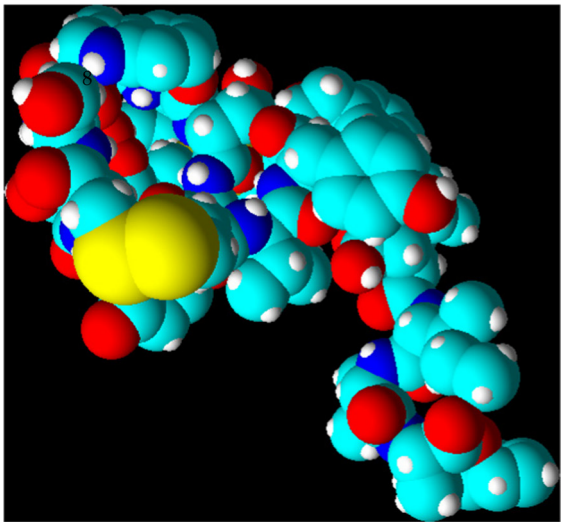

d)

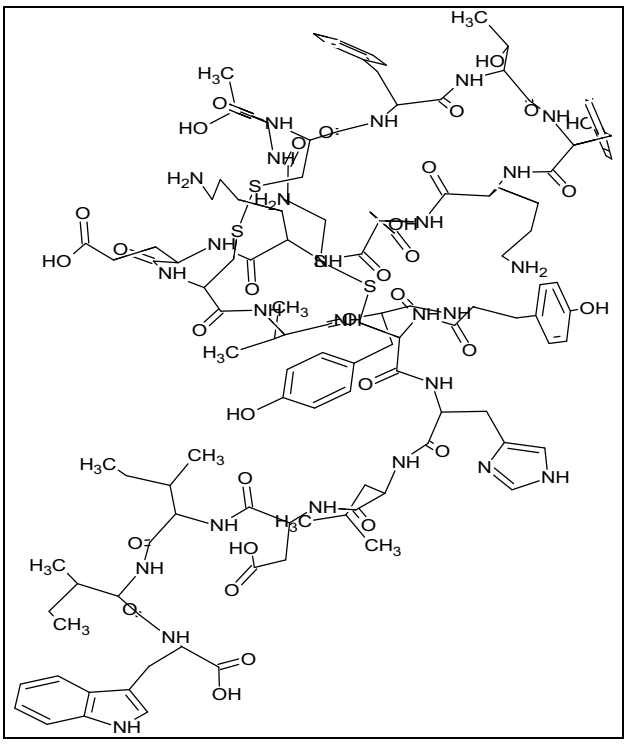

e)

f)

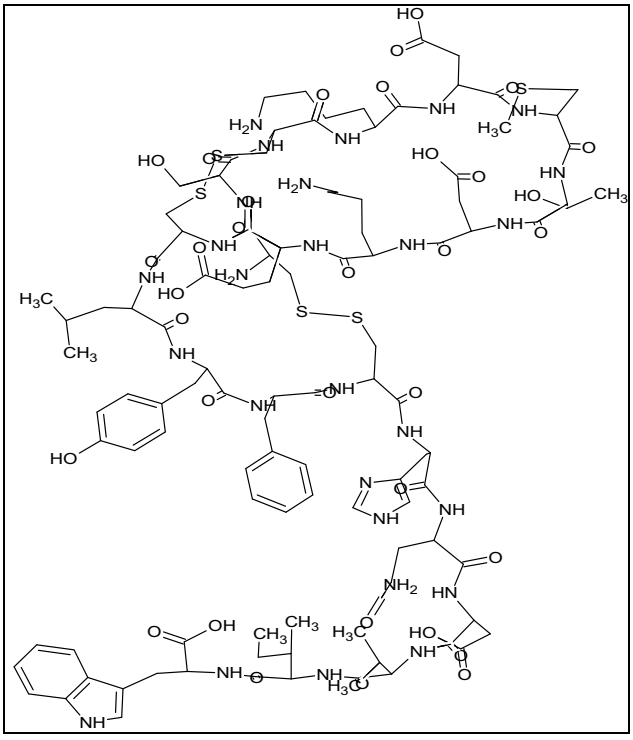

g)

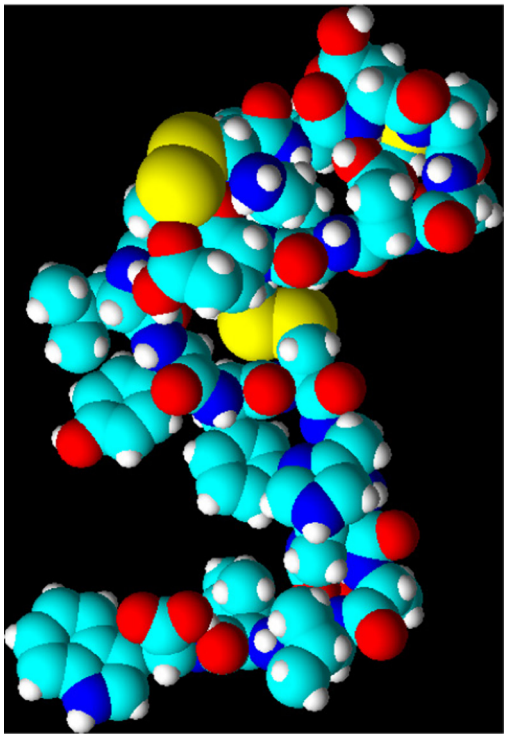

h)

**Figure 3:** Structures of ETs and SRT-6b; (a) ET-I and (b) ET-I space-filling model; (c) ET-II and (d) ET-II space-filling model; (e) ET-III and (f) ET-III space-filling model; (g) SRT-6b and (h) ET-III space-filling model; all structures and models are minimum energy conformers. Structures are shown without explicit hydrogens, the space-filling models' explicit hydrogens are white.

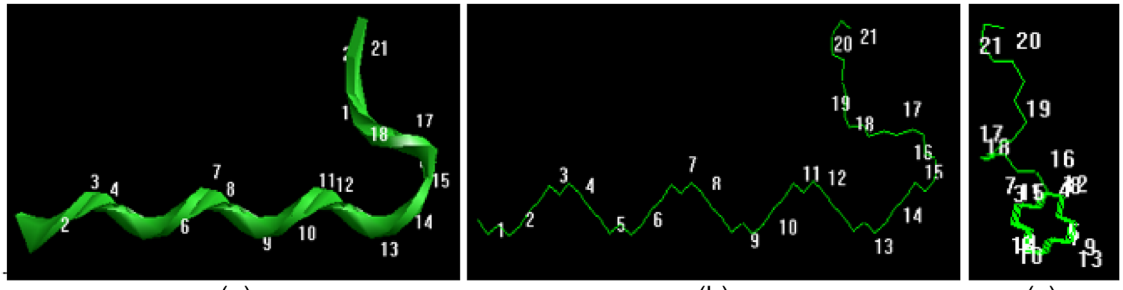


**Figure 4:** Endothelin, ET-I; (a and b) back-bone models (no S–S bonds); (c) a cavity-like loop formed between AA 1–15 where in AA 16–21 are not participating in the loop formation (all structures are at minimum energy conformations MEC, optimized geometry).

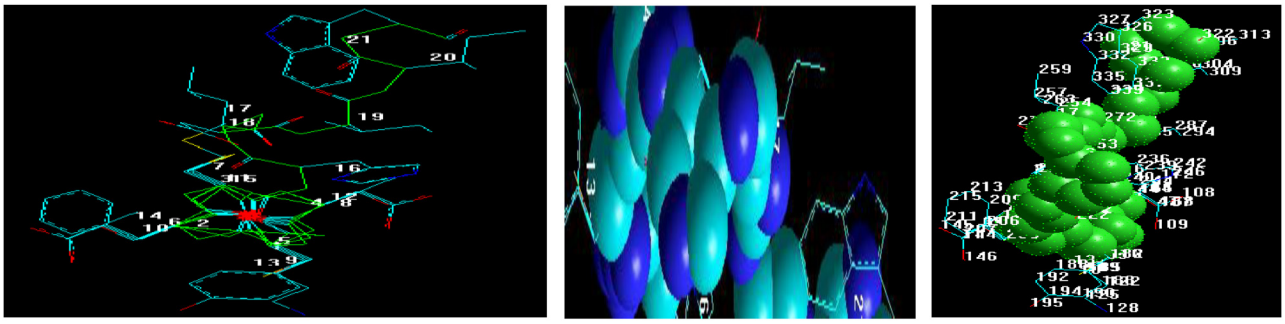


**Figure 5:** ET-I model backbone views; (a) backbone holding the side structures, loop area, and backbone atoms seen in green color; (b) backbone as ball-model holding the residues; (c) residue atoms distribution around backbone's green model.

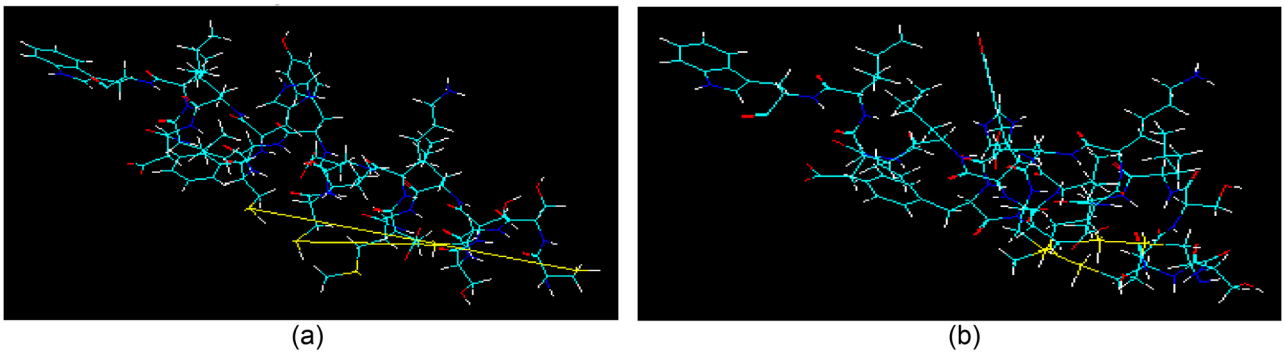


**Figure 6:** ET-I Models and S–S bonds formation: (a) ET-I model cyclized between AA, Cys–Cys at 1–15, and 3–11 of sulfur residues (yellow connections), cyclization bonding shown as two yellow lines; (b) an energy minimized model of A after 5,100 cycles, Monte-Carlo simulations, the S–S bond lengths reduced and two cyclic loops generated.

played a part in the compartmentalization. The distribution along the axes 1–2 and 3–4 indicated that the ET-I tail (AA 16–21) together with AAs positioned at 13,14, and 15 forms the distinct distribution part as equal weightage with the counterpart of the distribution, the two Cys–Cys cyclizations (AA 1–15 and 3–11) and the residue 12 (Figure 7). The exclusivity of the chain is also exhibited in the electrostatic potential and total charge distribution (Figure 8), which is localized in the non-tail part of the ET-I structure. This also may help to refute the notion of the cyclic part (AA 1–15) being inactive as this part has more pronounced electron density, charge distribution, and consequently prone to chemical/biochemical interaction with energy requirements to be active.

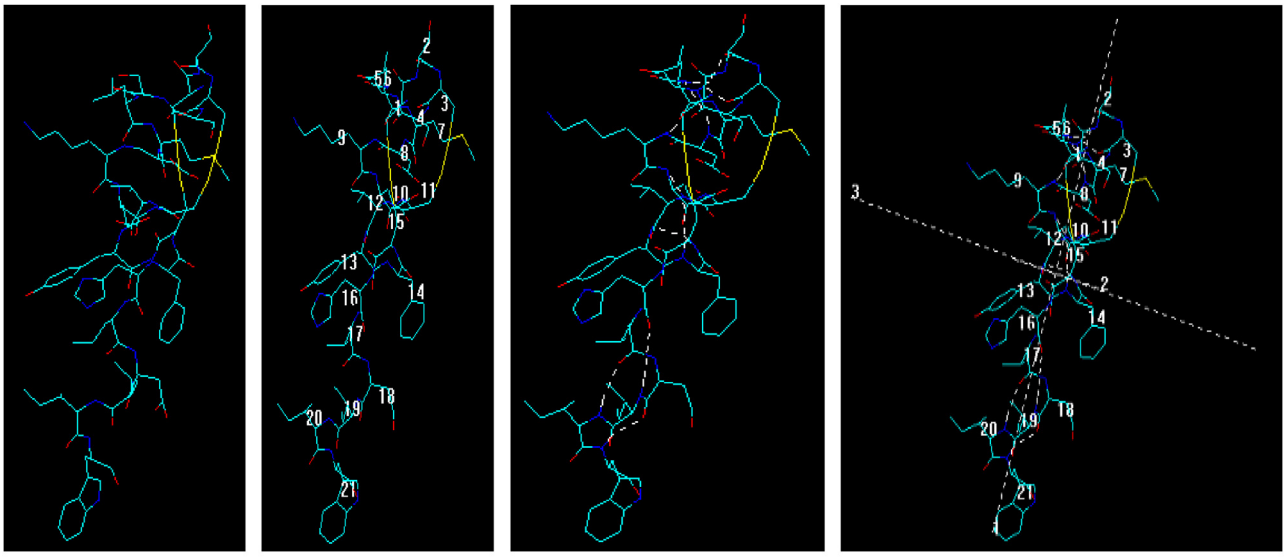


**Figure 7:** ET-I model without explicit hydrogens and S–S bonds; (a) ET-I model, MEC; (b) AA residues identified after cyclization between AA Cys–Cys 1–15 and Cys–Cys 3–11; (c) facilitated hydrogen-bondings between residues, shown as broken white lines; (d) atoms and residues distribution weightage shown along the dotted lines on the internal axes from 1–2 and 3–4 of other than hydrogen-bondings broken lines of the residues (for hydrogen-bondings refer to model c).

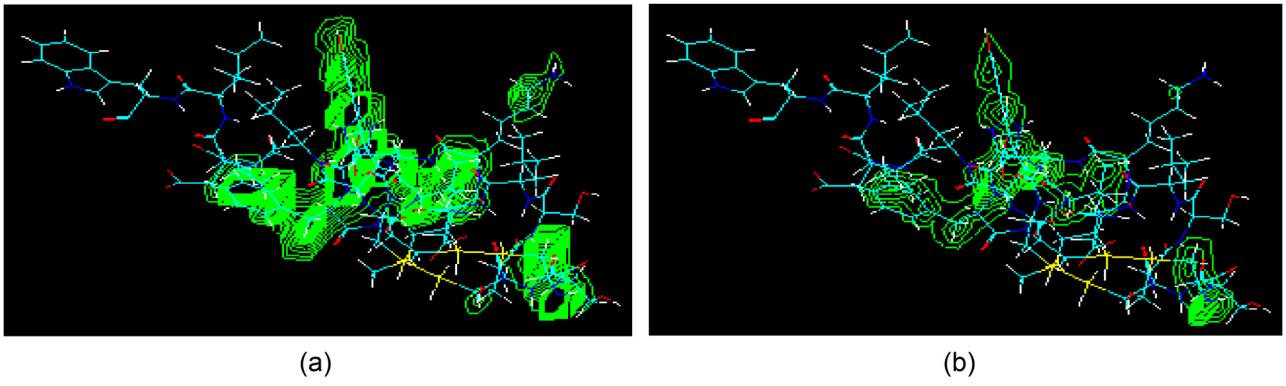


**Figure 8:** ET-I: electrostatic potential and charge density; (a) electrostatic potential on the ET-I molecule after dual cyclization, a 2D representation; (b) total charge density presented as 2D contours, dense lines represent strong influences.

## 3.7 Prototypical template, sequence analysis, and replaceable tail: Generation of new chemical entity

The ETs without tails are a bicyclic structure identified as cyclic structures, A and B, with S–S bonds between two Cys units at positions 3 and 11, and at positions 1 and 15, together with the interconnecting atoms and bonds of the peptidic structure between them. One cyclic unit contains 8 AAs identified as sequence $Cys^{1}$–Ser–$Cys^{3}$–$Cys^{11}$–Val–Tyr–Phe–$Cys^{15}$ with S–S bonds between AA 1 and 15, and AA 3 and 11. The other unit constituted of 9 AAs identified as a sequence $Cys^{3}$–Ser–Ser–Leu–Met–Asp–Lys–Glu–$Cys^{11}$ with S–S bonds between 3 and 11. The two structures are deduced after $Cys^{3}$ and $Cys^{11}$ positions taken as common between both the cyclic parts. The addition of tail from either ETs, or from the SRT-6b provided two mini ET prototypical templates. Another combination making an interesting structural subtype for the monocyclic mini ET ring is produced by the modeling of ET-I, which constituted 12 AAs identified in sequence as $Cys^{3}$–$Cys^{11}$–$Val^{12}$–$Tyr^{13}$–$Phe^{14}$–$Cys^{15}$–$His^{16}$–$Leu^{17}$–$Asp^{18}$–$Ile^{19}$–$Ile^{20}$–$Trp^{21}$ incorporating the hexapeptide tail with AAs from 16–21 with Cys–Cys S–S bond between AA at positions 3 and 11. In an attempt to partially open the ET-I

structure, the AA linkages between AAs at positions 3 and 4 were cleaved to give rise to two tail like structures linked to AAs 11 and 15.

The original hexapeptide side chain was intact in its attachment to the $Cys^{15}$ AA as viewed on the ET-I models. The additional side chain thus generated contained AA $Ser^{4}$ to $Glu^{10}$ linked sequentially, and joined to the monocyclic structure at $Cys^{11}$. Thus, the monocyclic ring comprised of AA $Cys^{1}$–$Ser^{2}$–$Cys^{3}$–$Cys^{11}$–$Val^{12}$–$Tyr^{13}$–$Phe^{14}$–$Cys^{15}$. The shortening of the cyclic sub-structure contained the AA identified in the backbone of ET-I, where side chain is tail-ender in both the cases. However, an analysis on the majority of the occurrences of AA in ET-I revealed that the Cys (at 4 positions, *i.e.*, 1, 3, 11, and 15) is the most common AA followed by the Ser(3), Leu(2), Asp(2), and Ile(2) where Ile, found 2 times, is specific to the hexapeptide tail chain. The sequence derived could be Cys–Ser–Leu–Asp–Cys conjoined by S–S bond between first and last Cys residues. A 3D analysis of ET-I showed the concentration of aromatic ring containing AA in one domain probably facilitating the binding [78]. The sequence can be modified to include the hexapeptide chain with the most common AA sequence Cys–Ser–Leu–Asp–Cys and with the sequence Cys–Ser–Leu–Asp–Cys–Ileu, although the change in hexapeptide constitution is not favorable and is not recommended keeping in view of the homology with other ETs tails (AA 16–21), *i.e.*, ET-II, and ET-III.

The differential biological activity of ET-II and ET-III are different and their receptor affinity separate with ET-II have certain cross-affinity. The fact that the ET-II has only two different AAs (Trp at 6, and Leu at position 7) as compared with the ET-I, while the ET-III have a total of 6 different AAs, of which all the 6 are of the non-tail part, and localized in the cyclic structure part of the ET-III, as compared to the ET-I. The AA differentiation has contributory roles in the receptor affinity of the three distinct ETs, through the interactions at the molecular and atomic levels. The AA occurrence criteria and repeating sequence observations for these AA provided Cys–Ser–Trp–Leu–Asp–Cys as the other template for ET-II with the common ETs hexapeptide side chain (AA 16–21) attached. The Cys–Ser–Trp–Leu–Asp–Cys–Ile is the other sequence analyzed for its analogy for the ET-II sequence shortening as a ligand for probably being binding facilitator. The ET-III analysis produced the AA sequences Cys–Thr–Phe–Tyr–Lys–Cys, Cys–Thr–Phe–Tyr–Lys–Asp–Cys and Cys–Thr–Phe–Tyr–Lys–Asp–Cys–Ile with the common hexapeptide chain where both the Cys' are joined by S–S bonds to give the monocyclic structures. The energy profile and conformational analysis put the sequences in similar category of physico-chemical parameters. The AAs Asp and Ile in the proposed common AA-based sequences can be deleted *in lieu* of the hexapeptide chain attachment. The extra Cys was provided for the S–S linkage. The SRT-6b hexapeptide tail is also an important sequence moiety needing evaluation in the changed structural domains, and in the sequence shortening exercise with the detailed biological evaluation for these sequences is necessary in future.

## 3.8 Cys AA combinations and further shortening of the ETs: New and shortened sequences

The Cys combinations can be tried for further shortening of the long sequences of the ETs. The first approach was keeping the Cys residues as $Cys^{1}$–$Ser^{2}$–$Cys^{3}$–$Cys^{11}$–$Cys^{15}$ with S–S bonds between $Cys^{1}$–$Cys^{15}$ and $Cys^{3}$–$Cys^{11}$ with the hexapeptide tail from the ETs. The further shortening can give Cys–Ser–Cys with S–S bonds between both the Cys residues, and any one of the Cys residues attaching the common hexapeptide side chain from the ETs. The sequence for ET-I and SRT-6b based moiety will be of interest to compare as there exists lesser commonality between them. The ET-III have different AA sequences than the ET-I, whereby the ET-III differs in a total of six AAs and all of them are in the non-tail part of the structure. The ET-III is also considerably different in its AA constituents as compared to the ET-II molecule. The structural differences speak for the varying molecular properties, QSAR values (Table 1), and consequently the differences in the receptor type affinity. The ET-III was distinctly different than the ET-I, and seemingly was more close to the SRT-6B structure. The AA commonality and differences, and their respective physico-chemical evaluation, and biological activity response profile as well as the effects of the shortened sequences are worth deliberating. The ET-I sequence in another combination approach provided $Cys^{3}$–$Cys^{11}$–$Val^{12}$–$Tyr^{13}$–$Phe^{14}$–$Cys^{15}$ and $Cys^{\forall}$–$Val^{12}$–$Tyr^{13}$–$Phe^{14}$–$Cys^{15}$ with S–S bonds between Cys residues in analogy to the ET-I ($Cys^{1}$–$Cys^{15}$, $Cys^{3}$–$Cys^{11}$), between $Cys^{1}$–$Cys^{15}$, between $Cys^{3}$–$Cys^{15}$, and between $Cys^{3}$–$Cys^{11}$ as derived from the ET-I sequence with the hexapeptide attached. The changeover of the S–S bond relationship in ET-I to $Cys^{1}$–$Cys^{11}$ and $Cys^{3}$–$Cys^{15}$ provided the sequence as Cys–Cys–Cys-hexapeptide tail, and Cys–Ser–Cys–Cys-hexapeptide tail with feasible S–S bonds between the Cys residues. The non-hydrophilic AA *in lieu* of Cys residue in S–S linkage cross-over model can also be tried. The AAs can be Ala, Val, Leu, and Pro.

The cyclic part of the ET-I will give the Cys–Ser–Val–Tyr–Phe–Cys, Ser–Cys–Val–Tyr–Phe–Cys, Cys–Tyr–Phe–Cys from the substructure $Cys^{1}$–$Ser^{2}$–$Cys^{3}$–$Cys^{11}$–$Val^{12}$–$Tyr^{13}$–$Phe^{14}$–$Cys^{15}$ and Cys–Ser–Leu–Met–Asp–Lys–Glu–Cys, Ser–Leu–Met–Asp–Cys–Glu with S–S bonds between terminal Cys, and amide linkage in last example between Cys and Glu from the ET-I substructure $Cys^{3}$–$Ser^{4}$–$Ser^{5}$–$Leu^{6}$–$Met^{7}$–$Asp^{8}$–$Lys^{9}$–$Glu^{10}$–$Cys^{11}$. The hexapeptide chain from ETs and SRT-6b as tail attachments at the carboxyl and N-terminal have also been analyzed for their molecular attributes and conformational analysis. The dissecting approach to ET-I producing various shorter peptides is depicted in Figure 9. The generated structures, S1–S18, were estimated for their molecular and QSAR properties (Table 2). The electrostatic potential and charge density were observed as high, moderate, and low in nature based on their intensity expressed as eccentric lines in high, low, and medium densities with localizations/distributions on the structures. Among the high exhibits of the electrostatic potentials were the structures S1, S4, S5, S8, S9, S12, S13, S14, S15, S16, and S17, Bosentan, Mecitentan, and other antagonists, *e.g.*, BQ-123, 485, and 788, while the medium

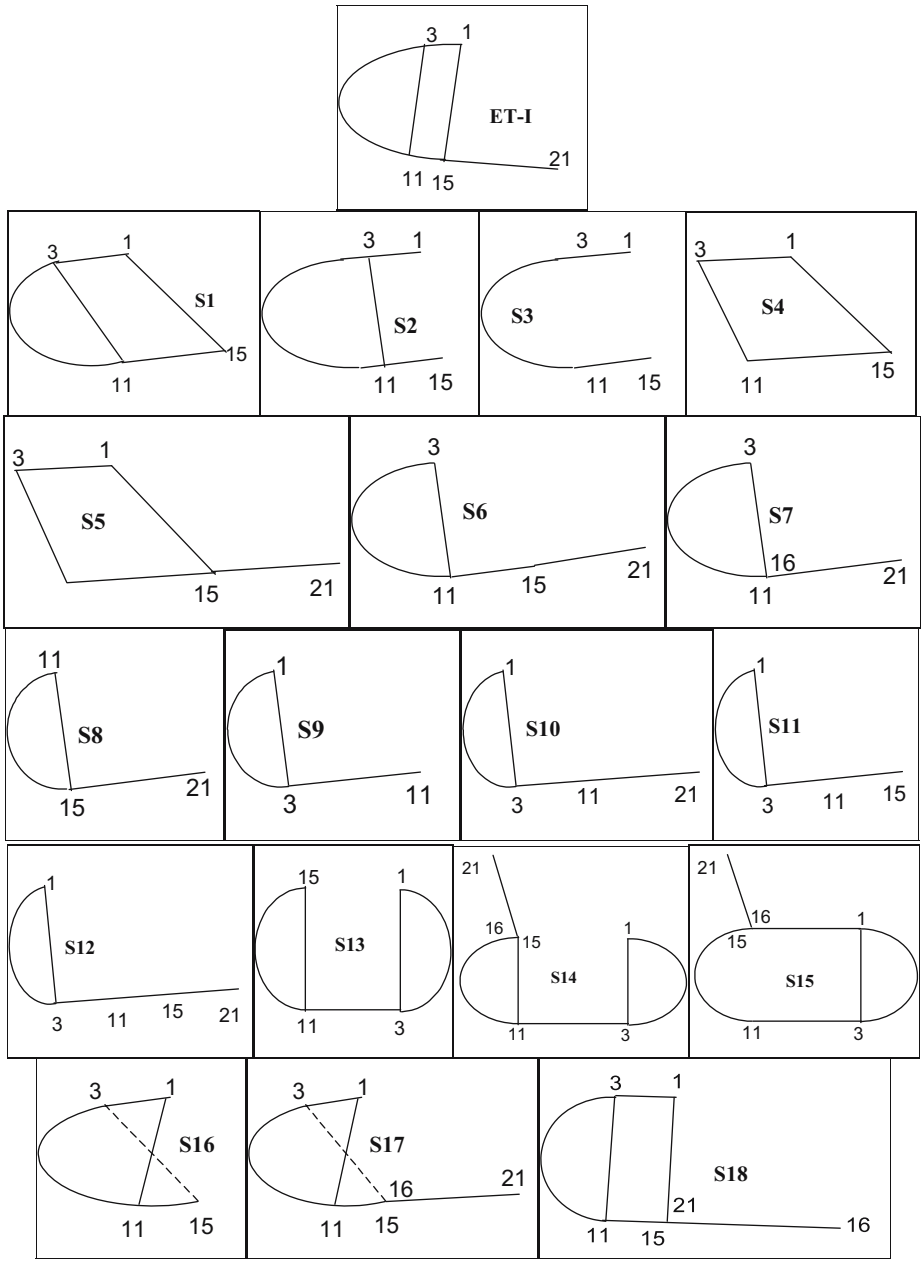


**Figure 9:** ET-I: structure dissecting approach, all AAs represented by a number are continuous natural chain of ET-I unless stated in the figure, all Cys–Cys S–S bonds are straight lines unless otherwise stated; for figures S16, and S17, the broken lines represent the S–S bonds between the two Cys residues, $Cys^{3}$–$Cys^{15}$.

**Table 2:** Molecular attributes and QSAR properties of the ETs and SRT-6b derived structures (S1–S18)

| Molecular properties | S1 | S2 | S3 | S4 | S5 |
|---|---|---|---|---|---|
| Molar refractivity | 442.55 | 447.39 | 431.31 | 251.82 | 458.17 |
| Molar volume | 1,378.50 | 1,195.65 | 1,247.20 | 677.65 | 1,243.95 |
| Log *P* | 1.14 | 0.71 | 0.28 | −1.49 | 3.46 |
| Hydration energy | −38.37 | −39.87 | −44.08 | −17.37 | −31.34 |
| Parachor | 3,637.90 | 3,668.60 | 3,550.14 | 2,036.50 | 3,733.86 |
| Index of refraction | 1.555 | 1.671 | 1.608 | 1.665 | 1.6580 |
| Surface tension | 48.4.0 | 88.65 | 65.63 | 81.55 | 81.15 |
| Density | 1.283 | 1.48 | 1.370 | 1.45 | 1.41 |
| Polarizability | 175.44 | 177.36 | 170.98 | 99.83 | 181.63 |
| RBDE | 33 | 32 | 31 | 17 | 33 |

| Molecular properties | S6 | S7 | S8 | S9 | S10 |
|---|---|---|---|---|---|
| Molar refractivity | 606.76 | 468.86 | 371.14 | 287.85 | 494.28 |
| Molar volume | 1,819.20 | 1,428.60 | 1,098.80 | 862.10 | 1,463.30 |
| Log *P* | 7.72 | 6.12 | 5.84 | 1.06 | 4.02 |
| Hydration energy | −48.67 | 14.51 | −27.06 | −19.09 | −44.63 |
| Parachor | 4,992.66 | 3,892.26 | 3,019.96 | 2,460.66 | 4,157.90 |
| Index of refraction | 1.581 | 1.570 | 1.590 | 1.582 | 1.590 |
| Surface tension | 56.70 | 55.03 | 57.00 | 66.33 | 65.13 |
| Density | 1.296 | 1.292 | 1.282 | 1.395 | 1.353 |
| Polarizability | 240.54 | 185.87 | 147.13 | 114.11 | 195.95 |
| RBDE | 46 | 34 | 30 | 14 | 30 |

| Molecular properties | S11 | S12 | S13 | S14 | S15 |
|---|---|---|---|---|---|
| Molar refractivity | 425.75 | 632.19 | 426.75 | 633.10 | 625.33 |
| Molar volume | 1,252.7 | 1,853.90 | 1,152.55 | 1,715.35 | 2,000.50 |
| Log *P* | 0.67 | 5.66 | 0.02 | −3.31 | −2.27 |
| Hydration energy | −45.12 | −49.51 | −44.18 | −46.28 | −36.44 |
| Parachor | 3,561.06 | 5,258.34 | 3,530.46 | 5,227.66 | 5,179.76 |
| Index of refraction | 1.595 | 1.597 | 1.662 | 1.659 | 1.537 |
| Surface tension | 65.20 | 64.70 | 88.05 | 86.25 | 44.90 |
| Density | 1.369 | 1.345 | 1.48 | 1.45 | 1.236 |
| Polarizability | 168.78 | 250.62 | 169.18 | 250.98 | 247.90 |
| RBDE | 26 | 42 | 27 | 43 | 44 |

| Molecular properties | S16 | S17 | S18 | ET-Tail ($AA^{16-21}$) | SRT-6b-Tail ($AA^{16-21}$) |
|---|---|---|---|---|---|
| Molar refractivity | 423.06 | 629.50 | 423.06 | 209.95 | 204.29 |
| Molar volume | 1,355.8 | 1,957.0 | 1,355.8 | 622.13 | 589.53 |
| Log *P* | −1.09 | 3.86 | 5.76 | 4.54 | 1.72 |
| Hydration energy | −39.95 | −37.50 | −56.19 | −14.46 | −19.11 |
| Parachor | 3,530.40 | 5,227.6 | 3,530.4 | 1,721.7 | 1,678.94 |
| Index of refraction | 1.536 | 1.556 | 1.536 | 1.590 | 1.609 2 |
| Surface tension | 45.90 | 50.9 | 45.9 | 58.60 | 65.73 |
| Density | 1.264 | 1.273 | 1.264 | 1.279 | 1.351 |
| Polarizability | 167.71 | 249.55 | 167.71 | 83.23 | 80.99 |
| RBDE | 27 | 43 | 27 | 16 | 17 |

were S2, S6, S7, S10, S11, and S18, and the low was S3. The charge intensity and localizations were high in S1, S6, S9, S10, S12, and S14, and medium levels were exhibited by S2, S4, S15, and S18, and Bosentan, Mecitentan, and other antagonists, while the low levels of the charge density were found in the structures S2, S3, S5, S7, S8, S10, S11, S13, S16, and S17. A closer look favored the high electrostatic potential with low to moderate/medium levels of charge density. This favored the structures S4 and S15, while other considerations were made to include other structures too (Figure 10).

## 3.9 Characteristics of the tail chain (AA 16–21) of ETs and SRT-6b

The ETs common tail (Figure 11) chain comprising the hexapeptide (AA 16–21, His–Leu–Asp–Ile–Ile–Trp, HLDIIW, single letter code sequence) and the SRT-6b hexapeptide (AA 16–21, His-Gln–Asp–Val–Ile–Trp, HQDVIW) were compared for their molecular properties and the QSAR values (Table 2). The major differences in the properties were observed in the log *P* values (ETs chain: 4.54 and SRT-6B chain: 1.72), hydration energies (ETs chain: –1,446 kcal/mol and SRT-6b chain: –1,911 kcal/mol), and molar volume (ETs chain: 622.13 $Å^{303}$ and SRT-6b chain: 589.53 $Å^3$)

The mutation approach of replacing the AA were utilized to further dwell upon the characteristic changes in the substructures and ETs (ET-I, II, and III) were provided with the SRT-6b tails (AA 16–21, His-Gln–Asp–Val–Ile–Trp), as well as the SRT-6b was attached with the replaced tail of the ETs. The QSAR and molecular properties estimation (Table 3) showed that the ET-III and SRT-6b produced characteristics in the same range, while the ET-I and ET-II were of the same league in their molecular properties, especially the log *P* and hydration energy together with the refractivity.

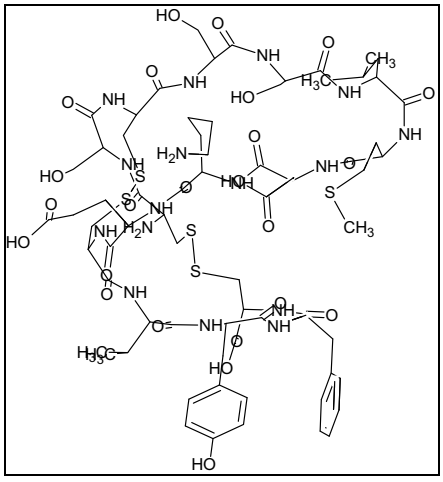

a)

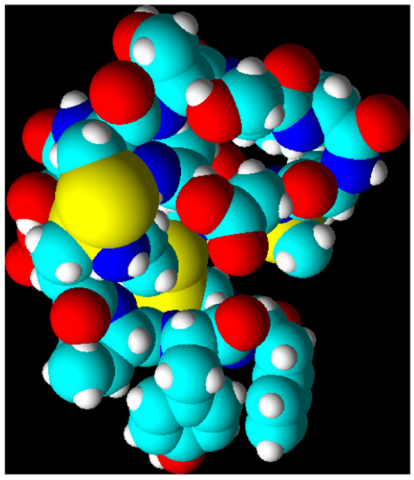

b)

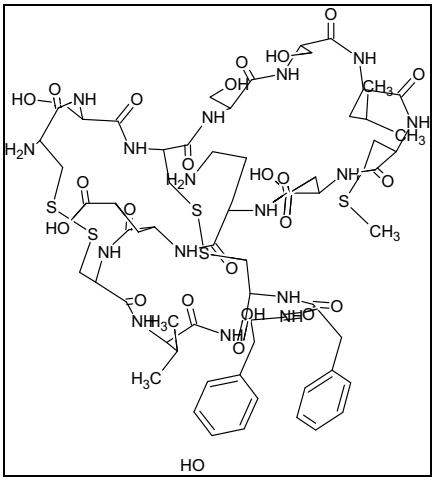

c)

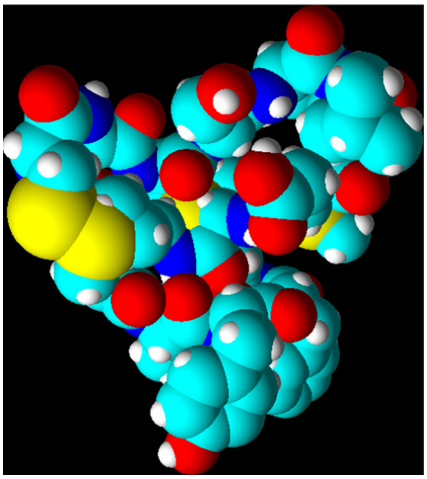

d)

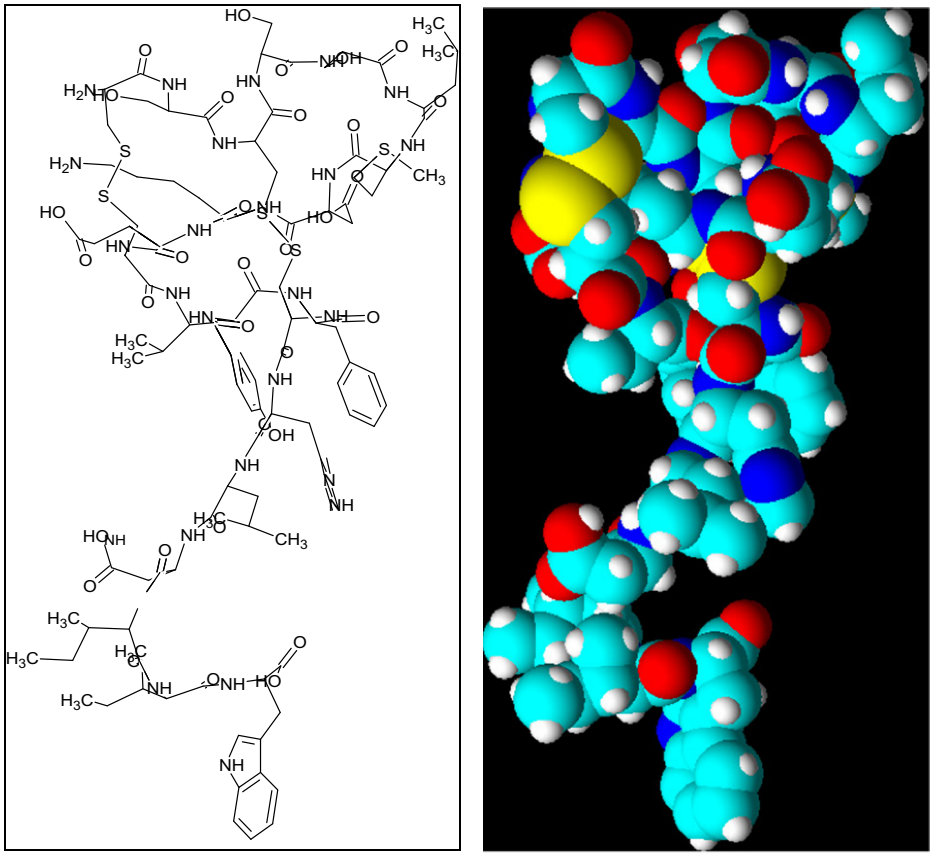

e) f)

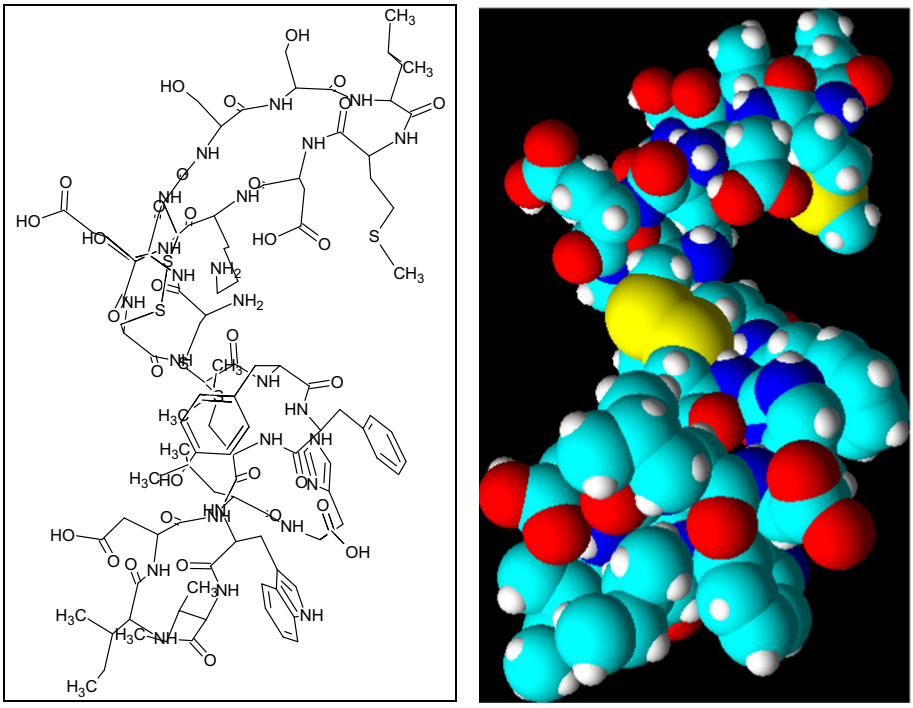

g) h)

**Figure 10:** ET-I derived structures; structures of: (a) S1 (AA 1–15 and 3–11 Cys–Cys S–S bonds) and (b) S1 space-filling model; unusual Cys–Cys bonds (AA 1–11 and 3–15 Cys–Cys) models; (c) S16 and (d) S16 space-filling model; (e) S17 (AA 1–11 and 3–15 Cys–Cys S–S bonds) and (f) S17 space-filling model; (g) S18 (AA 1–15 and 3–11 Cys–Cys S–S bonds and the Tail chain AA 16–21 is attached as reversed sequence, AA 21–16 = Tyr–Ile–Ile–Asp–Leu–His), and (h) S18 space-filling model. All structures are shown without explicit hydrogens, the models' explicit hydrogens are white.

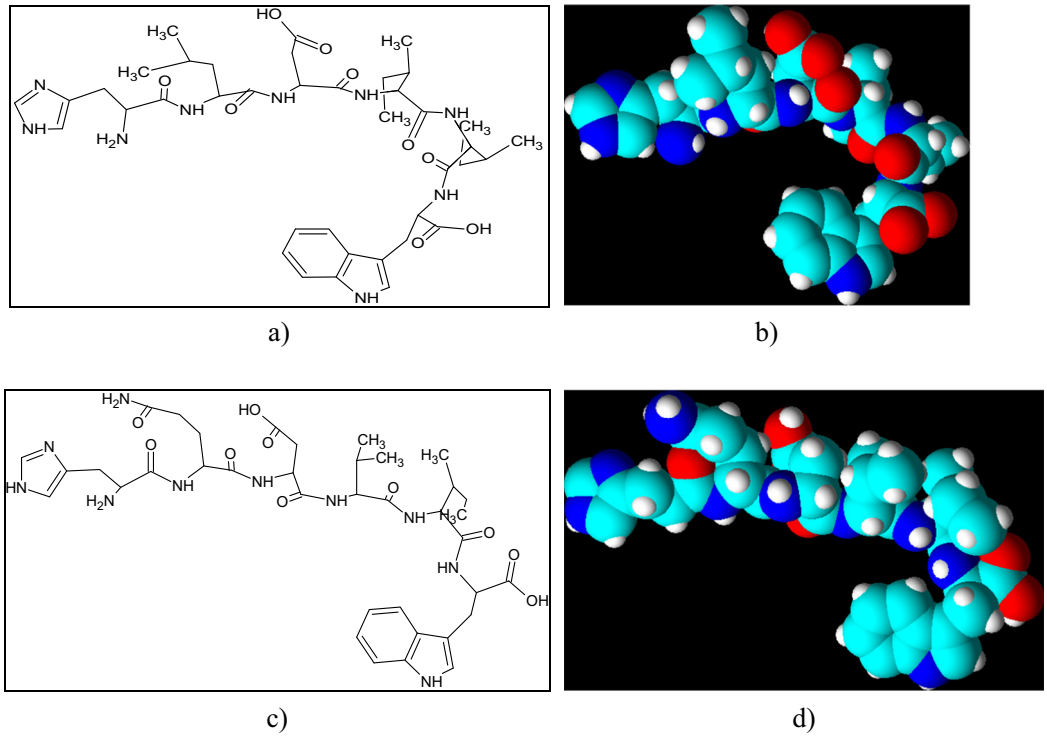


**Figure 11:** Tail chain structures (AA 16–21); (a) ETs tail chain structure (without explicit hydrogens shown); (b) ETs chain structure space-filling model; (c) SRT-6b chain structure (without explicit hydrogen atoms shown); (d) SRT-6b chain structure space-filling model.

The mutant structures have also been designed and some of the mutant points for ETs have been identified through NMR analysis and that confirms the existence of mutants [79].

## 3.10 Comparative study of the properties: Antagonists evaluation

The molecular properties and the QSAR values estimation of the model ET-I antagonists, Bosentan, Mecitentan (Figure 12), BQ-123, BQ-485, and BQ-788 were carried out (Table 4).

The studied antagonists have a range of log *P* values, hydration energies from lowest (–6.38 kcal/mol) to highest (0.28 kcal/mol) and differing molecular sizes. The values have importance in their range which entails that the very high molecular and QSAR property values are for the high molecular weight (MW) products, and that the low MW products designed on the ETs structural analysis can also be potent and selective based on the SPR relationship when compared with the known antagonists.

However, for the designated products and the ETs, there were ranges of log *P* from 4–9 and hydration energies between 40 and 60 kcal/mol that were observed for the ETs structures. The designed chemical entities were expected to fall in this range for probable bioactivity as ET-I antagonist. Nonetheless, the log *P* values and the hydration energies were in the ranges of 1–7 and –13.50–0.28 kcal/mol, respectively, for the known antagonists (Table 4). The ET-I derived

**Table 3:** ETs hexapeptide tails mutation: SPR observations

| Molecular properties | ET-I (AA 1–15) with SRT-6b Tail (AA 16–21) | ET-II (AA 1–15) with SRT-6bTail (AA 16–21) | ET-III (AA 1–15) with SRT-6b Tail (AA 16–21) | SRT-6b (AA 1–15) with ETs-Tail (AA 16–21) |
|---|---|---|---|---|
| Molar refractivity | 209.95 | 204.29 | 608.83 | 622.67 |
| Molar volume | 622.13 | 589.53 | 1,537.44 | 1,994.94 |
| Log *P* | 4.54 | 4.72 | 5.10 | 5.45 |
| Hydration energy | –14.46 | –19.11 | –57.35 | –54.80 |
| Polarizability | 83.23 | 80.99 | 254.07 | 254.15 |

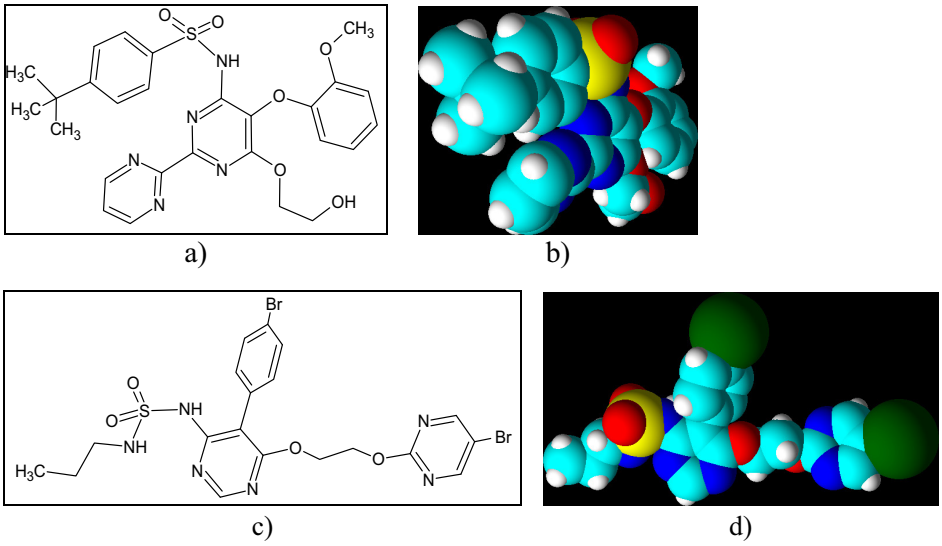


**Figure 12:** Structures of the ET-I antagonists: (a) Bosentan (without explicit hydrogens); (b) Bosentan space-filling model; (c) Mecitentan; and (d) Mecitentan space-filling model.

and designed compounds were expected to exhibit these value ranges. Some of the designed structures, S1–S4, were near in the desired geometric shape and size range in accordance with the antagonistic molecules, while the structures S16–18 were near to the ET-I. The structures, S5–S12, were in the intermediate ranges of the size and shape as compared to the ET-I. The QSAR and the molecular properties comparison also indicated these preferences, and the structures, S2, S4, S11, S14, S15, and S16, seemed near the mother ET, ET-I, in comparative outcome of the analysis, although the variations in the properties were pronounced as compared to the molecular shape, size, and the presence of double bonds equivalents, together with the other properties of parachor, hydration energy, polarizability, *etc.* (Table 2).

## 3.11 Vesiculation: A plausible approach

The functions and transport of different biomolecules may require nano-vesiculation that is considered safe for transport, stability, and supposedly works as dynamic entity to perform physiological functions of inherent and dictated nature at the transported site. Protection against cytosolic calcium ions overload in cellular stress conditions and cell injury are also known to be maneuvered through vesiculaation at nanoscale of the membranes. A rapid vesiculation of peptidic molecules have also been suggested. The surroundings, structural, and physico-chemical properties led compartmentalization due to selective constrictions in the structural network producing reduced volume of the structure may further tend to minimize size and molecular weight and geometry characteristics leading towards generation of vesiculation. The structural compartmentalization, compartments of geo-spatial changes, seemed to be an outcome of several factors, including asymmetric presence of calcium ion [80–83]. The interconnected open structural parts formed as the final, or intermediate shape as tubular entities, which enables the free diffusion of proteins and calcium ions [84] can be a format for structural change. Nonetheless, the structural integrity and intrinsic characteristics to retain and preserve the primary structure puts the peptidic

**Table 4:** Molecular and QSAR properties of the known ET-I antagonists

| Molecular properties | Bosentan | Macitentan | BQ-123 | BQ-485 | BQ-788 |
|---|---|---|---|---|---|
| Molar refractivity | 143.69 | 125.55 | 155.26 | 173.91 | 165.21 |
| Molar volume | 416.0 | 351.2 | 618.79 | 592.10 | 762.95 |
| Log *P* | 1.06 | 3.21 | 4.67 | 3.26 | 6.96 |
| Hydration energy | −13.49 | −2.61 | −6.38 | −4.41 | 0.28 |
| Polarizability | 56.96 | 49.77 | 63.81 | 70.47 | 65.35 |

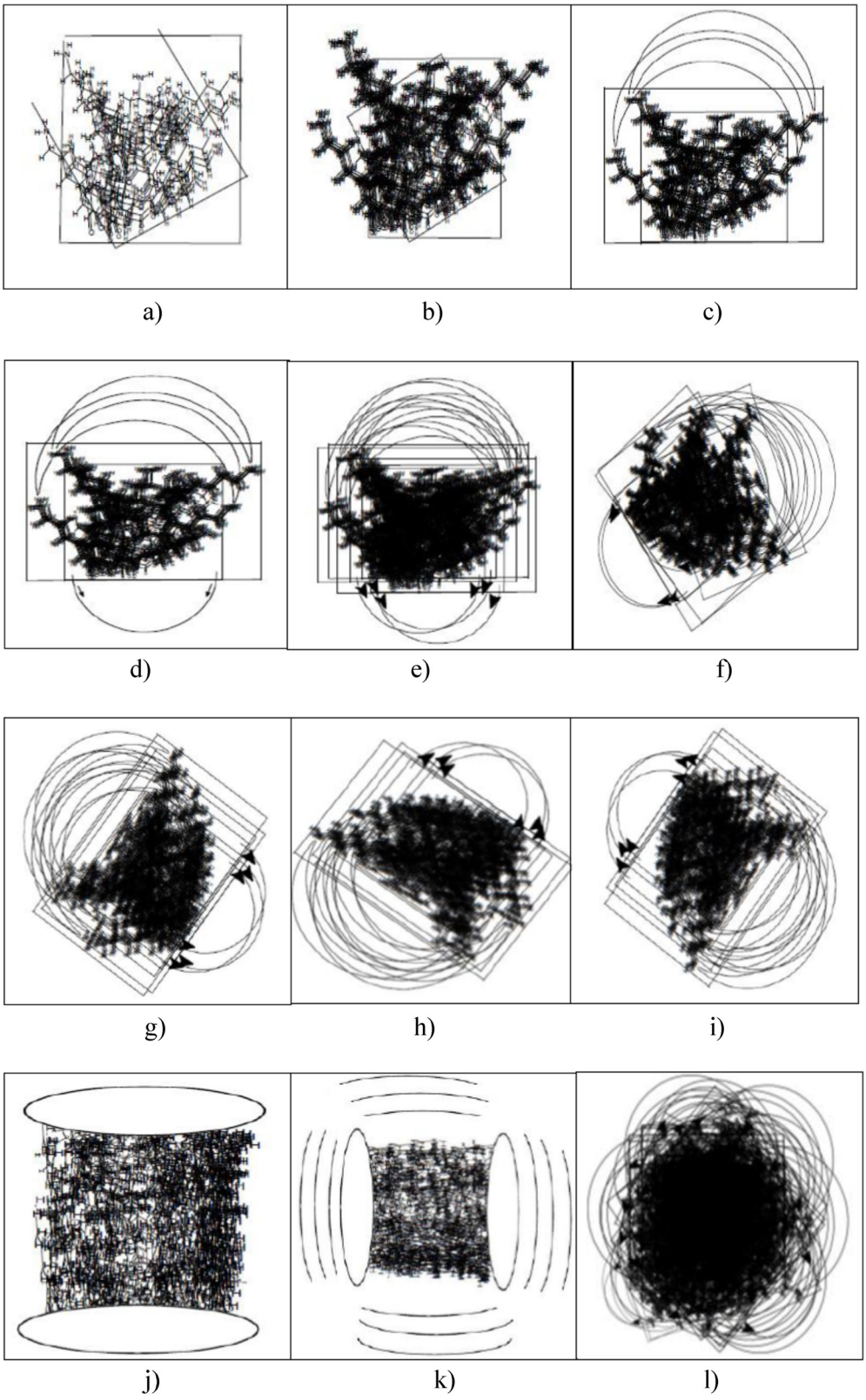


**Figure 13:** Plausible approach to nano-vesiculation; (a) surface interaction; (b) interfacial activity; (c) single-dimension interaction; (d) another dimension based interaction and structural motifs assembly; (e) increased interaction; (f) twisting of the structural motifs' direction; (g–i) multi-directional increased movements and interactions; (j) lateral compression of the assembled structural motifs; (k) compression leading to volume reduction, and counter-compression yielding to increased interfacial interactions, and further compression and reduction of volume; (l) formation of a prototypical nano-vesicle, entrapping ions, water molecule, and small molecular weight entities.

molecules in an altered and preferred shape, a vesicle, or a hollow spherical cage retaining some ions, water, and other surrounding small molecular weight entities [85–92]. These vesicles can be nano-sized based on the peptidic structure size and molecular weight, as well as their proneness to be nano as dictated by the molecular and physico-chemical interactions, and the role of surroundings and surface in contact. The growing nanostructures may go through the compartmentalization of the molecular area based on their physical interactions towards a tube-like structure, or a cavitation to give the supramolecular structure of assembled peptidic structures of diminished size which are prone to more intense, multi-cornered interactions and that may tend to be rounding and layering through assembly and collection of many peptidic structures with their irregular and haphazard interactions among themselves to produce an ultimate vesicular form [81].

Additionally, the factors which tend to vesiculize the peptidic structures, including surface interactions within itself and other entities, especially of lipidic nature, hydrogen-bonding and presence of hydrophobic groups and their interactions, energy requirements, initiation to geometrical prototype development and dip for curvature, compartmentalization, backbone layering of the molecular templates under the influence of physico-chemical forces, and interactions as peptide nanostructures lead through endogenously self-initiated, and self-assembled, and contributed by the thiol reactivity of proteinic cysteines are suggested [93,94]. However, the self-assembly in lipidic surroundings preferentially led to small nano-disk formation of the polypeptide molecules, and the nano-disks are thermodynamically favorable [95,96]. Experimentally, as recently reported [97,98], the surface roughness retards the molecular stretching, and geometric folding to provide diminished crystallinity for certain polymeric nanostructures, and any untoward attempt to crystallize the peptidic structure seemingly leads to vesicle formation with the growth of the nano-mass till its critical/threshold size is reached, also controlled by the factors of surface, surroundings, and intrinsic physico-chemical interactions of the developing nano-structure. The interactive, interfacial assembled peptides are prone to vesiculation which is suggested to be either generated through formation of nano-disks which comparatively are more energy preferred [89,99–101], or alternatively through different route. The protein-based structures follow the lead of the other self-assembled bio-nanostructures, *e.g.*, DNA and RNA. The self-assembled virus complex encapsulate and transport the viral DNA for host cell delivery. The natural polypeptides of 20 AAs with differing properties, and a minimum of 4 structurally similar nucleotides have been found to introduce towards forming the nanostructures [102]. Vesicular shapes self-assembled from folded and globular protein molecules, and under aqueous media, as well as thermally-triggered self-assembled vesicles with roles from different factors, including the interfacial interactions among the polymeric structures that is strong for lipidic vesicles preparation, and the other parameters, *i.e.*, phase transition, hydrogen bonding, hydrophilicity, electrostatic repulsion, hydrophobic interactions, changes in the surface area of the layer, and lateral pressure in initiating the vesiculation have also been suggested [103–105].

The vesiculation steps are predicted based on the physico-chemical interactions, surroundings, and resultant structural changes [86] including generation of passage for transport, or other activities. These activities may happen within seconds to provide needed passage, protection, and lead to the formation of different shapes, preferably as a vesicle, or a spherical cage (Figure 13) [87–105]. The energy in solvation, hydrophilic attractions, systemic and cellular components interactions, repetitions in structure, presence of ions, zwitterionic and dipolar nodes, and size-limitation (nano-cut) at structural/atomic scales, and the stability requirements catapult the longer biopolymeric structures to nano-shaping.

## 4 Conclusion and prospects

ETs and SRT-6b structural analyses generated sequences of shorter AA lengths with the molecular attributes and QSAR properties, of which some matching the original ET sequence. Certain sequences were *in silico* generated through different approaches of molecular analysis which showed promising molecular properties *at par* with the mother ET which can be developed to be utilized as ET antagonist. More advanced functional analysis of ETs structures' through various approaches and methodology and synthesis of the ETs-derived structures awaits, which is not only for evaluating additional pharmacological studies using the specifically designed ET antagonists, but also generation of genetically altered animal models for testing, especially rodents, owing to the feasibility and observations that the majority of ET-based design and biotesting studies have been performed on the rodent models. The bioactivity evaluation as an approach where conditional loss-of-biofunction(s) and gain-of-biofunction(s) manipulations to check the hypothesis is desired. Studies in feasibility, mechanism, process, and simulations for vesiculation of ETs, including big ET, together with their property and biofunctions need to be experimentally studied.

**Acknowledgements:** The authors thank their colleagues for helpful discussions.

**Funding information:** The authors state no funding involved.

**Author contributions:** All authors have accepted responsibility for the entire content of this manuscript and approved its submission.

**Conflict of interest:** The authors state no conflict of interest.

## References

[1] Boulpaep EL, Boron WF. Medical physiology: a cellular and molecular approach. 2nd International edition. Philadelphia, PA, USA: Saunders/Elsevier; 2009. p. 480. ISBN 9781437720174, ISBN 1-4160-3115-4.

[2] Furchgott RF, Zawadzki JV. The obligatory role of endothelial cells in the relaxation of arterial smooth muscle by acetylcholine. Nature. 1980;288:373–6.

[3] Davenport AP, Morton AJ, Brown MJ. Localization of endothelin-1 (ET-I), ET-II, and ET-III, mouse VIC, and sarafotoxin S6b binding sites in mammalian heart and kidney. J Cardiovas Pharmacol. 1991;17(Suppl 7):S152–5.

[4] Hickey KA, Rubanyi GM, Paul RJ, Highsmith RF. Characterization of a coronary vasoconstrictor produced by cultured endothelial cells. Am J Physiol. 1985;248:C550–6.

[5] Gillespie MN, Owasoyo JO, McMurtry IF, O'Brien RF. Sustained coronary vasoconstriction provoked by a peptidergic substance released from endothelial cells in culture. J Pharmacol Exp Ther. 1986;236:339–43.

[6] O'Brien RF, Robbins RJ, McMurtry IF. Endothelial cells in culture produce a vasoconstrictor substance. J Cell Physiol. 1987;132:263–70.

[7] Masaki T. The discovery of endothelins. Cardiovasc Res. 1998;39:530–3.

[8] Yanagisawa M, Kurihara H, Kimura S, Tomobe Y, Kobayashi M, Mitsui Y, et al. A novel potent vasoconstrictor peptide produced by vascular endothelial cells. Nature. 1988;332:411–5.

[9] Inoue A, Yanagisawa M, Kimura S, Kasuya Y, Miyauchi T, Goto K, et al. The human endothelin family: three structurally and pharmacologically distinct isopeptides predicted by three separate genes. Proc Natl Acad Sci USA. 1989;86:2863–7.

[10] Schneider MP, Boesen EI, Pollock DM. Contrasting actions of endothelin ET(A) and ET(B) receptors in cardiovascular disease. Annu Rev Pharmacol Toxicol. 2007;47:731–59.

[11] Sakurai T, Yanagisawa M, Masaki T. Molecular characterization of endothelin receptors. Trends Pharmacol Sci. 1992;13:103–8.

[12] Jae HS, Winn M, von Geldern TW, Sorensen, Chiou BK, Nguyen WJ, Marsh B, et al. Pyrrolidine-3-carboxylic acids as endothelin antagonists. 5. Highly selective, potent, and orally active ETA antagonists. J Med Chem. 2001;44:3978–84.

[13] Boss C, Bolli MH, Weller T, Fischli W, Clozel M. Bis-sulfonamides as endothelin receptor antagonists. Bioorg & Med Chem Lett. 2003;13:951–4.

[14] Neidhart W, Breu V, Burri K, Clozel M, Hirth G, Klinkhammer U, et al. Discovery of Ro 48-5695: a potent mixed endothelin receptor antagonist optimized from bosentan. Bioorg Med Chem Letts. 1997;7:2223–8.

[15] Harada H, Kazami J, Watanuki S, Tsuzuki R, Sudoh K, Fujimori A, et al. Ethene sulfonamide and ethane sulfonamide derivatives, a novel class of orally active endothelin-A receptor antagonists. Bioorg Med Chem. 2001;9:2955–68.

[16] Bolli MH, Boss C, Clozel M, Fischli W, Hess P, Weller T. The use of sulfonylamido pyrimidines incorporating an unsaturated side chain as endothelin receptor antagonists. Bioorg Med Chem Lett. 2003;13:955–9.

[17] He GW, Liu MH, Yang Q, Furnary A, Yim APC. Role of endothelin-1 receptor antagonists in vasoconstriction mediated by endothelin and other vasoconstrictors in human internal mammary artery. Annals Thoracic Surgery. 2007;84:1522–7.

[18] Dasgupta F, Mukherjee AK, Gangadhar N. Endothelin receptor antagonists-an overview. Curr Med Chem. 2002;9:549–75.

[19] Langlois C, Létourneau M, Lampron P, St-Hilaire V. Development of agonists of endothelin-1 exhibiting selectivity towards ETA receptors. Fournier A. Br J Pharmacol. 2003;139:616–22.

[20] Kiowski W, Sutsch G, Hunziker P, Muller P, Kim J, Oechslin E, et al. Evidence for endothelin-1-mediated vasoconstriction in severe chronic heart failure. Lancet. 1995;358:732–6.

[21] Shihoya W, Nishizawa T, Okuta A, Tani K, Dohmae N, Fujiyoshi Y, et al. Activation mechanism of endothelin ETB receptor by endothelin-1. Nature. 2016;537:63–8.

[22] Cheng XM, Lee C, Klutchko S, Winters T, Reynolds EE, Welch KM, et al. Synthesis and structure activity relationships of a 9-substituted acridine as endothelin-A receptor antagonists. Bioorg Med Chem Lett. 1996;6:2999–3002.

[23] Ishizuka N, Matsumura K, Sakai K, Fujimoto M, Mihara S, Yamamori T. Structure-activity relationships of a novel class of endothelin-A receptor antagonists and discovery of potent and selective receptor antagonist, 2-(benzo[1,3]-dioxol-5-yl)-6-isopropyloxy-4-(4-methoxyphenyl)-2H-chromene-3-carboxylic acid (S-1255). 1. Study on structure-activity relationships and basic structure crucial for ET (A) antagonism. J Med Chem. 2002;45:2041–55.

[24] Harada H, Kazami J, Watanuki S, Tsuzuki R, Sudoh K, Fujimori A, et al. Synthesis and structure–activity relationships in a series of ethenesulfonamide derivatives, a novel class of endothelin receptor antagonists. Chem Pharm Bull. 2001;49:1593–603.

[25] Lättig J, Oksche A, Beyermann M, Rosenthal W, Krause G. Structural determinants for selective recognition of peptide ligands for endothelin receptor subtypes $ET_A$ and $ET_B$. J Pept Sci. 2009;15:479–91.

[26] Niiyama K, Takahashi H, Nagase T, Kojima H, Amano Y, Katsuki K, et al. Structure–activity relationships of 2-substituted 5,7-diaryl cyclopenteno[1,2-b]pyridine-6-carboxylic

acids as a novel class of endothelin receptor antagonists. Bioorg Med Chem Lett. 2002;12:3041–5.
[27] Barton M, Yanagisawa M. Endothelin: 20 years from discovery to therapy. Can J Physiol Pharmacol. 2008;86:485–98.
[28] Vignon-Zellweger N, Heiden S, Miyauchi T, Emoto N. Endothelin and endothelin receptors in the renal and cardiovascular systems. Life Sci. 2012;91:490–500.
[29] Kedzierski RM, Yanagisawa M. Endothelin system: the double-edged sword in health and disease. Annu Rev Pharmacol Toxicol. 2001;41:851–76.
[30] Uchida Y, Ninomiya H, Saotome M, Nomura A, Ohtsuka M, Yanagisawa M, et al. Endothelin, a novel vasoconstrictor peptide, as potent bronchoconstrictor. Eur J Pharmacol. 1988;154:227–8.
[31] Kohan DE. Endothelin-1 and hypertension: from bench to bedside. Curr Hyperten Rep. 2008;10:65–9.
[32] Schneider MP, Mann JF. Endothelin antagonism for patients with chronic kidney disease: still a hope for the future. Neph Dial Transplant. 2014;29:i69–73.
[33] Emoto N, Vignon-Zellweger N, Lopes RA, Cacioppo J, Desbiens L, Kamato D, et al. 25 years of endothelin research: the next generation. Life Sci. 2014;118:77–86.
[34] Bradley EK, Ng SC, Simon RJ, Spellmeyer DC. Synthesis, molecular modelling, and NMR structure determination of four cyclic peptide antagonists of endothelin. Bioorg Med Chem. 1994;2:279–96.
[35] Cucarull-González JR, Laggner C, Langer T. Influence of the conditions in pharmacophore generation, scoring, and 3D database search for chemical feature-based pharmacophore models: one application study of ETA- and ETB-selective antagonists. J Chem Inf Model. 2006;46:1439–55.
[36] Iqbal J, Sanghia R, Das SK. Endothelin receptor antagonists: an overview of their synthesis and structure-activity relationship. Mini Rev Med Chem. 2005;5:381–408.
[37] Cody WL, He JX, DePue PL, Waite LA, Leonard DM, Sefler AM, et al. Structure-activity relationships of the potent combined endothelin-A/endothelin-B receptor antagonist Ac-DDip16–Leu–Asp–Ile–Ile–Trp21: development of endothelin-B receptor selective antagonists. J Med Chem. 1995;38:2809–19.
[38] Spellmeyer DC, Brown S, Stauber GB, Geysen HM, Valerio R. Endothelin receptor ligands. Multiple D-amino acid replacement net approach. Bioorg Med Chem Lett. 1993;3:1253–6.
[39] Spellmeyer DC, Brown S, Stauber GB, Geysen HM, Valerio R. Endothelin receptor ligands. Replacement net approach to SAR determination of potent hexapeptides. Bioorg Med Chem Lett. 1993;3:519–24.
[40] Compeer MG, Suylen DPL, Hackeng TM, De Mey JGR. Endothelin-1 and -2: two amino acids matter. Life Sci. 2012;91:607–12.
[41] Shihoya W, Nishizawa T, Yamashita K, Inoue A, Hirata K, Kadji FMN, et al. X-ray structures of endothelin ETB receptor bound to clinical antagonist bosentan and its analog. Nat Struct Mol Biol. 2017;24:758–64.
[42] Galie N, Olschewski H, Oudiz RJ, Torres F, Frost A, Ghofrani HA, et al. Ambrisentan for the treatment of pulmonary arterial hypertension: results of the ambrisentan in pulmonary arterial hypertension, randomized, double-blind, placebo-controlled, multicenter, efficacy (ARIES) study 1 and 2. Circulation. 2008;117(23):3010–9.
[43] Filep JG, Rousseau A, Fournier A, Sirois P. Structure-activity relationship of analogues of endothelin-1: dissociation of hypotensive and pressor actions. Eur J Pharmacol. 1992;220:263–6.
[44] Galoppini C, Giusti L, Macchia M, Hamdan M, Mazzoni MS, Calvani F, et al. Synthesis and structure–activity relationship studies of new endothelin pseudopeptide analogues containing alkyl spacers. Il Farmaco. 1999;54:213–17.
[45] Murugesan N, Gu Z, Stein PD, Spergel S, Bisaha S, Liu ECK, et al. Biphenylsulfonamide endothelin receptor antagonists. Part 3: structure–activity relationship of 4′-heterocyclic biphenyl sulfonamides. Bioorg Med Chem Lett. 2002;12:517–20.
[46] Kanda Y, Kawanishi Y, Oda K, Sakata T, Mihara S, Asakura K, et al. Synthesis and structure–activity relationships of potent and orally active sulfonamide ETB selective antagonists. Bioorg Med Chem. 2001;9:897–907.
[47] Morimoto H, Shimadzu H, Hosaka T, Kawase Y, Yasuda K, Kikkawa K, et al. Modifications and structure–activity relationships at the 2-position of 4-sulfonamidopyrimidine derivatives as potent endothelin antagonists. Bioorg Med Chem Lett. 2002;12:81–4.
[48] von Geldern TW, Kester JA, Bal R, Wu-Wong JR, Chiou W, Dixon DB, et al. Azole endothelin antagonists. 2. Structure-activity studies. J Med Chem. 1996;39:968–81.
[49] von Geldern TW, Hoffman DJ, Kester JA, Nellans HN, Dayton BD, Calzadilla SV, et al. 3. Using delta log *P* as a tool to improve absorption. J Med Chem. 1996;39:982–91.
[50] von Geldern TW, Hutchins C, Kester JA, Wu-Wong JR, Chiou W, Dixon DB, et al. 1. A receptor model explains an unusual structure-activity profile. J Med Chem. 1996;39:957–67.
[51] Morimoto H, Fukushima C, Yamauchi R, Hosino T, Kikkawa K, Yasuda K, et al. Design, synthesis, and structure–activity relationships of indan derivatives as endothelin antagonists; new lead generation of non-peptidic antagonist from peptidic leads. Bioorg Med Chem. 2001;9:255–68.
[52] Dong J, Yang N, Liang Y, Wu P, Li X, Liu K. Design and structure-activity relationship of novel endothelin receptor a tripeptide antagonists. Inter J Pep Res Ther. 2005;11:125–9.
[53] Erhardt PW. Endothelin structure and structure-activity relationships. In: Rubanyi GM, editor. Endothelin. Clinical Physiology Series. Rockville, MD, USA: American Physiological Society; 1992. p. 41–57. doi: 10.1007/978-1-4614-7514-9-4. ISBN 978-1-4614-7514-9.
[54] Nakajima K, Kumagaye S, Nishio H, Kuroda H, Watanabe TX, Kobayashi Y, et al. Synthesis of endothelin-1 analogues, endothelin-3, and sarafotoxin S6b: structure-activity relationships. J Cardiovasc Pharmacol. 1989;;13(Suppl 5):S8–18.
[55] Nakajima K, Kubo S, Kumagaye S, Nishio H, Tsunemi M, Inui T, et al. Structure-activity relationship of endothelin: importance of charged groups. BBRC. 1989;163:424–49.
[56] Yu W-S, Zhao Y-F, Liang Y-J, Liu K-L, Fei G-S, Wang H. The chemical syntheses and bioactivities of novel peptide-based endothelin antagonists. J Pep Res. 2002;59:134–8.
[57] Kimura S, Kasuya Y, Sawamura T, Shimmi O, Sugita Y, Yanagisawa M, et al. Structure activity relationship of

endothelin: Importance of the C-terminal moiety. BBRC. 1988;156:1182–6.
[58] Macchia M, Barontini S, Ceccarelli F, Galoppini C, Giusti L, Hamdan M, et al. Toward the rational development of peptidomimetic analogs of the C-terminal endothelin hexapeptide: development of a theoretical model. Farmaco. 1998;53:545–6.
[59] Nagase T, Mase T, Fukami T, Hayama T, Fujita K, Niiyama K, et al. Linear peptide ETA antagonists: rational design and practical derivatization of N-terminal amino- and imino-carbonylated tripeptide derivatives. Bioorg Med Chem Lett. 1995;5:1395–400.
[60] Li X, Liu K-L, Zheng J-Q, Chi MG, Dong J, Dong SJ, et al. Pharmacological characterization of 3-azabicyclo [3, 2, 1] octane-1-yl-l-leucyl-d-tryptophanyl-d-4-Cl-phenylalanine: a novel ETA receptor-selective antagonist. Pulmon Pharmacol Ther. 2008;21:780–7.
[61] Neustadt B, Wu A, Smith EM, Nechuta T, Fawzi A, Zhang H, et al. A case study of combinatorial libraries: endothelin receptor antagonist hexapeptides. Bioorg Med Chem Lett. 1995;5:2041–4.
[62] Terrett N, Bojanic D, Brown D, Steele J. The combinatorial synthesis of a 30,752-compound library: discovery of SAR around the endothelin antagonist, FR-139,317. Bioorg Med Chem Lett. 1995;5:917–22.
[63] Ishikawa K, Ihara M, Noguchi K, Mase T, Mino N, Saeki T, et al. Biochemical and pharmacological profile of a potent and selective endothelin B-receptor antagonist, BQ-788. Proc Nat Aca Sci USA. 1994;91:4892–6.
[64] Hruby V. Designing peptide receptor agonists and antagonists. Nat Rev Drug Discov. 2002;1:847–58.
[65] Wink LH, Baker DL, Cole JA, Parrill AL. A benchmark study of loop modeling methods applied to G protein-coupled receptors. J Comput Aided Mol Des. 2019;33:573–95.
[66] Bellows-Peterson ML, Fung HK, Floudas CA, Kieslich CA, Zhang L, Morikis D, et al. De novo peptide design with C3a receptor agonist and antagonist activities: theoretical predictions and experimental validation. J Med Chem. 2012;55(9):4159–68.
[67] Manning M, Stoev S, Chini B, Durroux T, Mouillac B, Guillon G. Peptide and non-peptide agonists and antagonists for the vasopressin and oxytocin V1a, V1b, V2 and OT receptors: research tools and potential therapeutic agents. Prog Brain Res. 2008;170:473–512.
[68] Spinella MJ, Malik AB, Everit J, Andersen TT. Design and synthesis of a specific endothelin 1 antagonist: effects on pulmonary vasoconstriction. Proceed National Acad Sci USA. 1991;88(16):7443–6.
[69] Maggi CA, Giuliani S, Patacchini R, Santicioli P, Rovero P, Giachetti A, et al. The C-terminal hexapeptide, endothelin-(16-21), discriminates between different endothelin receptors. Eur J Pharmacol. 1989;166:121–2.
[70] Mahjoub Y, Malaquin S, Mourier G, Lorne E, Abou Arab O, Massy ZA, et al. Short- versus long-sarafotoxins: two structurally related snake toxins with very different *in vivo* haemodynamic effects. PLoS One. 2015;10(7):e0132864.
[71] Maggi CA, Giuliani S, Patacchini R, Santicioli P, Giachetti A, Meli A. Further studies on the response of the guinea-pig isolated bronchus to endothelins and sarafotoxin S6b. Eur J Pharmacol. 1990;176:1–9.
[72] Skolovsky M, Galron R, Kloog Y, Bdolah A, Indig FE, Blumberg S, et al. Endothelins are more sensitive than sarafotoxins to neutral endopeptidase: possible physiological significance. Proc Nat Acad Sci USA. 1990;87:4702–6.
[73] Ambar I, Kloog Y, Schvartz I, Hazum E, Sokolovsky M. Competitive interaction between endothelin and sarafotoxin: Binding and phosphoinositides hydrolysis in rat atria and brain. BBRC. 1989;158:195–201.
[74] Galron R, Bdolah A, Kochva E, Wollberg Z, Kloog Y, Sokolovsky M. Kinetic and cross-linking studies indicate different receptors for endothelins and sarafotoxins in the ileum and cerebellum. FEBS Lett. 1991;283:11–4.
[75] Cody WL, He JX, DePue PL, Rapundalo ST, Hingorani GP, Dudley DT, et al. Structure activity relationships in a series of monocyclic endothelin analogues. Bioorg Med Chem Lett. 1994;4:567–72.
[76] Yanagisawa M, Inoue A, Ishikawa T, Kasuya Y, Kimura S, Kumagaye S, et al. Primary structure, synthesis, and biological activity of rat endothelin, an endothelium-derived vasoconstrictor peptide. Proc Nat Acad Sci USA. 1988;85:6964–7.
[77] Smith NJ. Drug discovery opportunities at the endothelin B receptor-related orphan G protein-coupled receptors, GPR37 and GPR37L1. Front Pharmacol. 2015;6(275):1–13.
[78] Pletneva EV, Laederach AT, Fulton DB, Kostic NM. The role of cation-pi interactions in biomolecular association: design of peptides favoring interactions between cationic and aromatic amino acid side chains. J Am Chem Soc. 2001;123:6232–45.
[79] Dalgarno DC, Slater L, Chackalamannil S, Senior MM. Solution conformation of endothelin and point mutants by nuclear magnetic resonance spectroscopy. Inter J Pep Protein Res. 1992;40:515–23.
[80] Hunley TE, Kon V. Update on endothelins - biology and clinical implications. Pediat Nephrol. 2001;16:752–62.
[81] Subramanian M, Kielar C, Tsushima S, Fahmy K, Oertel G. DNA-mediated stack formation of nanodiscs. Molecules. 2021;26:1647.
[82] Subramanian K, Meyer T. Calcium-induced restructuring of nuclear envelope and endoplasmic reticulum calcium stores. Cell. 1997;89:963–71.
[83] Raval J, Góźdź WT. Shape transformations of vesicles induced by their adhesion to flat surfaces. ACS Omega. 2020;5(26):16099–100.
[84] Speksnijder JE, Terasaki M, Hage WJ, Jaffe LF, Sardet C. Polarity and reorganization of the endoplasmic reticulum during fertilization and ooplasmic segregation in the ascidian egg. J Cell Biol. 1993;120:1337–46.
[85] Jain SK, Yadava RK, Raikar R. Role of endothelins in health and disease. Indian Aca Clin Med J. 2002;3:59–64.
[86] Zohrabi T, Habibi N. Dendritic peptide nanostructures formed from self-assembly of di-l-phenylalanine extracted from Alzheimer's β-amyloid poly-peptides: insights into their assembly process. Inter J Pep Res Ther. 2015;21:423–31.
[87] Theil EC. Ferritin protein nanocages-the story. Nanotechnol Percept. 2012;8:7–16.
[88] Murata M, Narahara S, Kawano T, Hamano N, Piao JS, Kang J-H, et al. Design and function of engineered protein nanocages as a drug delivery system for targeting pancreatic cancer cells via neuropilin-1. Mol Pharmaceutics. 2015;12(5):1422–30.

[89] King NP, Bale JB, Sheffler W, McNamara DE, Gonen S, Gonen T, et al. Accurate design of co-assembling multi-component protein nanomaterials. Nature. 2014;510:103–8.
[90] Gradišar H, Jerala R. Self-assembled bionanostructures: proteins following the lead of DNA nanostructures. J Nanobiotech. 2014;12(4):1–9.
[91] Niemeyer CM, Mirkin CM, (Ed). Nanobiotechnology: concepts, applications, and perspectives: DNA–protein nanostructures. Germany: Wiley-VCH Verlag GmbH & Co; 2005. doi: 10.1002/3527602453.ch15.
[92] Yokoe H, Meyer T. Spatial dynamics of GFP-tagged proteins investigated by local fluorescence enhancement. Nature Biotech. 1996;14:1252–81.
[93] Shin K. Crystalline Structures, Melting, and Crystallization of Linear Polyethylene in Cylindrical Nanopores. Macromolecules. 2007;40(18):6617–23.
[94] Xue M, Cheng L, Faustino I, Guo W, Marrink SJ. Molecular mechanism of lipid nanodisk formation by styrene-maleic acid copolymers. Biophysical J. 2018;115(3):494–502.
[95] Jahn A, Stavis SM, Hong JS, Vreeland WN, DeVoe DL, Gaitan M. Microfluidic mixing and the formation of nanoscale lipid vesicles. Biophysical J. 2010;108:279–90.
[96] Jabbarzadeh A, Chen X. Surface-induced crystallization of polymeric nanoparticles: effect of surface roughness. Faraday Discussions. 2017;204:307–21.
[97] Boukouvala C, Daniel J, Ringe E. Approaches to modelling the shape of nanocrystals. Nano Convergence. 2021;8(1):26. doi: 10.1186/s40580-021-00275-6.
[98] Park WM, Champion JA. Thermally triggered self-assembly of folded proteins into vesicles. J Am Chem Soc. 2014;136(52):17906–9.
[99] Cheng G, Li W, Ha L, Han X, Hao S, Wan Y, et al. Self-assembly of extracellular vesicle-like metal-organic framework nanoparticles for protection and intracellular delivery of biofunctional proteins. J Am Chem Soc. 2018;140(23):7282–91.
[100] Monferrer A, Zhang D, Lushnikov AJ, Hermann T. Versatile kit of robust nanoshapes self-assembling from RNA and DNA modules. Nat Commun. 2019;10(1):608. doi: 10.1038/s41467-019-08521-6.
[101] Jang Y, Choi WT, Heller WT, Ke Z, Wright ER, Champion JA. Engineering globular protein vesicles through tunable self-assembly of recombinant fusion proteins. Small. 2017;13(36):1700399. doi: 10.1002/smll.201700399.
[102] Rangamani P, Mandadap KK, Oster G. Protein-induced membrane curvature alters local membrane tension. Biophysical J. 2014;107(3):751–62.
[103] Sodt AJ, Pastor RW. Molecular modeling of lipid membrane curvature induction by a peptide: more than simply shape. Biophysical J. 2014;106(9):1958–69.
[104] Bjørnestad VA, Orwick-Rydmark M, Lund R. Lipid nanodiscs formed by mixtures of styrene maleic acid (SMA) copolymers and lipid membranes. Langmuir. 2021;37:6178–88.
[105] Raeymaekers L, Larivière E. Vesicularization of the endoplasmic reticulum is a fast response to plasma membrane injury. BBRC. 2011;414:246–51.